Impact of softness on users' perception of curvature for future soft curvature-changing UIs

Zhuzhi Fan, Céline Coutrix

Impact of softness on users' perception of curvature for future soft curvature-changing UIs

Zhuzhi Fan
zhuzhi.fan@univ-grenoble-alpes.fr
CNRS, Université Grenoble-Alpes, LIG
Saint-Martin-d'Hères, France

Céline Coutrix
celine.coutrix@imag.fr
CNRS, Université Grenoble-Alpes, LIG
Saint-Martin-d'Hères, France

ABSTRACT

Soft (compliant) curvature-changing UIs provide haptic feedback through changes in softness and curvature. Different softness can impact the deformation of UIs when worn and touched, and thus impact the users' perception of the curvature. To investigate how softness impacts users' perception of curvature, we measured participants' curvature perception accuracy and precision in different softness conditions. We found that participants perceived the curviest surfaces with similar precision in all different softness conditions. Participants lost half the precision of the rigid material when touching the flattest surfaces with the softest material. Participants perceived all curvatures with similar accuracy in all softness conditions. The results of our experiment lay the foundation for soft curvature perception and provide guidelines for the future design of curvature- and softness-changing UIs.

CCS CONCEPTS

• **Human-centered computing → Empirical studies in HCI**.

KEYWORDS

Soft UIs, Shape-changing UIs, Psychophysics, Just Noticeable difference.

ACM Reference Format:
Zhuzhi Fan and Céline Coutrix. 2023. Impact of softness on users' perception of curvature for future soft curvature-changing UIs. In *Proceedings of the 2023 CHI Conference on Human Factors in Computing Systems (CHI '23), April 23–28, 2023, Hamburg, Germany*. ACM, New York, NY, USA, 19 pages. https://doi.org/10.1145/3544548.3581179

1 INTRODUCTION

Curved and soft materials gained increasing attention in the past decades in HCI [72]. The perception of the curvature of a soft surface comes into play, e.g., in virtual reality (VR) when a user is touching a surrounding daily object (e.g., a ball) to get haptic feedback [41], when a surgeon trains in VR with a soft organ proxy providing feedback through local curvature [61], when getting curvature-based shape notifications from a soft mobile device [97], or when soft physical buttons switch between different modes based on their curvature [40]. In these cases, the user experience is affected by the perceived curvature of the soft surface [1, 54].

https://doi.org/10.1145/3544548.3581179

Emerging technologies make it possible to actuate the curvature [52, 63, 97] and the softness [20] of UIs. To ensure the efficiency of such haptic feedback, HCI designers and researchers need to know users' ability to perceive the curvature of a soft UI. It is very important and timely to address this problem, as this is a bottleneck to ensure the efficiency of future interaction techniques [1, 72].

Based on prior work [10, 17, 19, 42, 65, 66, 77], we defined as *soft* the materials that have a Young's modulus[1] in the order of 10^4–10^6 Pa. Figure 1 shows that human fat, muscle, skin and silicone elastomer[2] are soft. Prior work studied the curvature perception of *rigid* objects [34, 35, 37, 55, 68, 71, 87–90, 92]. However, we do not know yet how well users perceive the curvature of *soft* objects, and whether the softness impacts the perception of the curvature. Yet, softness may have an impact on curvature perception, because both hard and curvy objects lead to a high response frequency of the same type of cutaneous mechanoreceptive afferent neurons [11, 36].

To design efficient haptic feedback with curvy and soft UIs, HCI designers particularly need to know users' *precision*, *accuracy* and *speed* when perceiving a change in the curvature of the soft UI. Users' precision is the minimum change in curvature of the soft UI that users can notice (Just Noticeable Difference or JND). Users' accuracy is the distance between the actual and perceived curvature (Point of Subjective Equality or PSE). Users' speed is the time users need to perceive the curvature of the soft UI (exploration time). This paper is the first to measure the impact of softness on users' precision, accuracy and speed when perceiving the curvature.

Our results reveal six new findings. First, users perceive our curviest surfaces (surface radius $R \approx 10mm$) as precisely (JND $\approx$ 0.63 mm) in different softness conditions. Second, users perceive our middle curved surfaces ($R \approx 20mm$) 25% more precisely in the two least soft conditions (JND $\approx$ 2mm) compared to the two softest conditions (JND $\approx 2.68mm$). Third, users perceive our least curved surfaces ($R \approx 40mm$) in the softest condition (JND= 8.61 mm) with half the precision of the rigid condition (JND= 4.31 mm). Fourth, users perceive curvier surfaces with better accuracy, from 2.67 mm to 0.31 mm. Fifth, users perceive surface curvature with similar accuracy in different softness conditions. Sixth, users perceive 17%

[1]The Young's modulus is a measure of the rigidity of materials. It is defined by the ratio between the lengthwise tension on a material and its change of length [21]. The larger the modulus, the more rigid the material.

[2]Durometer (Shore) hardness test is a commonly used hardness test for elastomeric materials. Durometer measurements assess the material's resistance to indentation, a higher durometer reading corresponds to a harder material. Different types of durometers have different hardness test ranges. A **Shore 00** durometer is typically used to test the hardness of extremely soft rubber, human and animal tissue; a **Shore 0** durometer is typically used to test the hardness of soft rubber and very soft plastics; a **Shore A** durometer is typically used to test the hardness of harder rubber, e.g., soft vulcanized rubber and natural rubber [22].

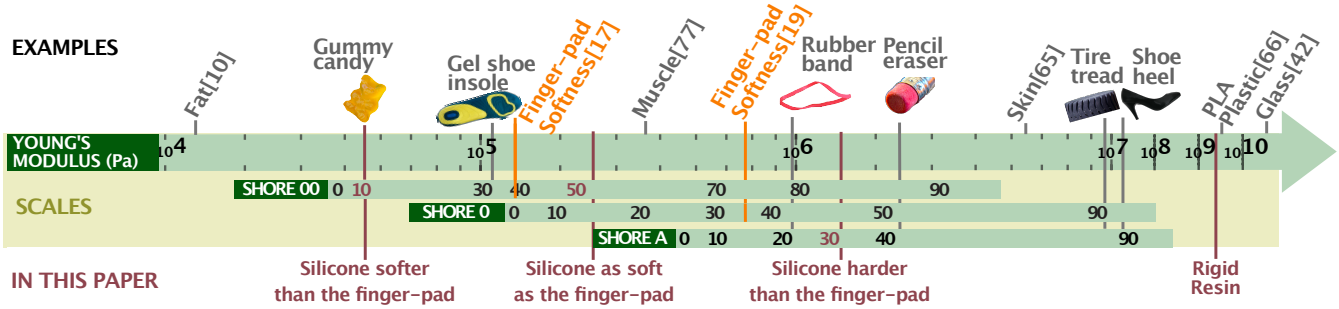

Figure 1: (Top) Example materials and objects and (center) their approximate Young's modulus [21] and respective Shore hardness [22]. (Bottom) Types of silicone and resin used in our experiment: Shore 00-10, Shore 00-50, Shore A-30, and Rigid.

slower all curvatures in the softest condition (3.95 s) compared to the rigid condition (3.39 s).

HCI designers can readily use the resulting guidelines for the design of efficient soft curvature-changing UIs. If feedback precision is crucial, designers should focus on very curved UIs ($R \approx 10mm$), where any softness can provide users with precise haptic curvature information. Alternatively, if designers need a larger range of curvatures, designers should change the stiffness to little rigid material (Shore A-30 in Figure 1). If feedback accuracy is crucial, designers should focus on very curved UIs ($R \approx 10mm$). Stiffening the material cannot improve the accuracy. If UIs need a high curvature refresh rate (e.g., $> 0.25Hz$), designers should use materials of softness >Shore 00-10 (Figure 1), and keep very soft curvature-changing UIs for a slower refresh rate.

2 RELATED WORK

Our work builds on top of previous work that studied users' psychophysical perception of curvature and softness.

2.1 Perception of curvature

Curvature can be perceived through cutaneous and kinesthetic cues. The cutaneous cues refer to the responses of mechanoreceptors [46] innervating the finger pad skin within and in the neighborhood of the contact area [54, 78]. The kinesthetic cues refer to the sense of position and motion of limbs, along with associated forces, conveyed by the sensory receptors in the skin around the joints, joint capsules, tedons and muscles [54, 78]. During passive touch, users only use cutaneous cues, while active touch [31] involves kinesthetic cues [54].

Passive touch. Goodwin et al. applied surfaces with different curvature as stimuli to participants' passive index finger with controlled force [34, 35]. They found that increasing the contact force (e.g., from 0.196 N to 0.588 N) could lead to participants' judging stimuli slightly less curved [34], and increasing the contact area (e.g., from 19.6 mm^2 to 53.6 mm^2) could slightly decrease participants' discrimination threshold [35]. Meanwhile, they found that both the effect of contact force [34] and contact area [35] were much smaller than the effect of surface curvature itself. They then used microneurography to record responses of tactile mechanoreceptors on participants' finger pads [36] when applying the same stimuli used in [34] to participants' passive index fingers. They found that the SAI afferents could well code the curvature information of stimuli for their steeply monotonically increasing response frequency to the stimuli curvature, whereas their response frequency increased slightly under larger contact force.

In short, with passive touch, which involves only cutaneous cues, participants can well discriminate surface curvature despite some slight bias induced by contact area and contact force.

Active touch. Gordon and Morison found participants' impressive performance when discriminating different curvatures with active touch [31]. They conducted several experiments [37] asking participants to use their index finger to actively explore the curvature of a graded series of surfaces produced using plano-convex lenses (diameter of 60 mm, step edge of 2 mm and base-to-peak height from 0 mm to 9.46 mm). They found participants could, in average, distinguish a lens with base-to-peak height of 0.09 mm from a lens with base-to-peak height of 0 mm (i.e. a flat lens).

Pont et al. found the effective stimulus for participants to discriminate surface curvature was the total height change over the surface (i.e., the ratio between the height and width of stimuli) when they slide a finger over it to explore the curvature [69]. This was confirmed by Louw et al. in their experiment measuring participants' detection thresholds for curvature in a larger range with stimuli having a Gaussian profile whose width (σ) ranges from 0.15 mm to 240 mm [55]. They found the discrimination threshold (i.e., stimulus height) of Gaussian-shaped stimuli increased with a power of 1.3 with increasing stimulus width. These work suggested that kinesthetic cues of participants' finger motion (e.g., the ratio of movement distance in the vertical and horizontal direction) can help participants to discriminate surface curvature.

Frisoli et al. conducted an experiment to confirm the important role of cutaneous cues during curvature perception [26]. Authors asked participants to discriminate the curvature of rendered virtual curved surfaces. These surfaces were rendered by a device providing haptic information (cutaneous and/or kinesthetic cues) at the fingertip. Their participants discriminated the curvature in two different conditions. (A) First, with *only kinesthetic cues*: participants inserted their finger into a thimble supported by a kinesthetic haptic device [9]. This device could provide users with kinesthetic cues by applying to the finger tip a force in the direction perpendicular to the virtual surface rendered. (B) Second, with *both kinesthetic and cutaneous cues*: during the exploration, an additional small mobile plate

supported by the same kinesthetic haptic device kept in contact with the finger tip. In addition to the previous kinesthetic cues, the plate could rotate instantaneously along the tangent to the point of contact between the finger and the virtual surface, to provide cutaneous cues informing about the shape geometry at the contact point. They found that with combined kinesthetic+cutaneous cues (B), participants were more precise: they had a 43% lower threshold for curvature discrimination compared to only kinesthetic cues.

In short, prior work found that users leverage both cutaneous and kinesthetic cues for curvature perception. However, their stimuli were either *rigid* curved objects (e.g., [34, 35, 37, 55, 69]), or rendered virtual curved surfaces with a *rigid* plate varying orientation (e.g., [26]). Consequently, these surfaces did not deform when the users' finger press on them. When touching a soft surface, the surface deformation can provide users with important cutaneous cues [5]. Meanwhile, the deformation will inversely change the local curvature of the surface. We need to further explore how this deformation caused by the surface softness will impact users' perception of the surface curvature. Such an information will ensure reliable haptic feedback to users of soft shape-changing interfaces.

2.2 Perception of softness

Srinivasan and LaMotte [78] studied the impact of cutaneous and kinesthetic cues on participants' perception of softness. They asked participants to discriminate the softness of flat stimuli made of rubber with 5 different levels of softness and in three conditions: (1) actively pressing with their middle finger on the stimuli; (2) actively pressing with their middle finger on the the stimuli with local cutaneous anesthesia; or (3) passively applying the stimuli on their middle finger pad with controlled contact force and speed. In condition 1, both cutaneous and kinesthetic cues were available to participants. In condition 2, only kinesthetic cues were available. In condition 3, only cutaneous cues were available. They found with only kinesthetic cues (2), participants' average discrimination accuracy decreased markedly (e.g., from $\geq$ 93% to $\leq$ 55% when discriminating between the softest stimuli and medium-soft stimuli). With only cutaneous cues (3), participants' average discrimination accuracy decreased much more slightly (e.g., from averagely 98% to averagely 93% when discriminating between the softest stimuli and the medium-soft stimuli). Their work revealed the critical role of cutaneous cues in softness discrimination.

According to Hertz's contact theory [45], the contact area of a finger with another soft surface increases as the finger presses deeper into the soft surface. This contact area increases more rapidly with a softer surface. Based on Hertz's contact theory, Bicchi et al. developed the Contact Area Spread Rate (CASR) device [6, 75] to provide participants with cutaneous information through the contact area between the finger and the device. The device varies its contact area with the user's finger pad, through a set of concentric cylinders of different radii in a telescopic arrangement. As the finger presses at the top of the system, it indents more deeply the cylinders. The finger gets in contact with the larger cylinders, enlarging the contact area. Bicchi et al. controlled the rate of the enlargement of the contact area according to the softness of the simulated surface: the softer the surface, the more rapidly the contact area increases as the finger presses on it. They found that with the cutaneous information provided by CASR, the participants had a similar success rate for the recognition of softness compared to real objects: 75% on average with CASR vs. 87% on average by directly exploring objects. This experiment further confirmed the important role of cutaneous cues, in particular the contact area, in softness discrimination.

Bergmann Tiest and Kappers conducted several softness estimation experiments using cutaneous and/or kinesthetic cues. They verified the vital contribution of cutaneous cues in softness discrimination (90% on average) and also show the less important contribution of kinesthetic cues (10% on average) [5].

Users take both kinesthetic and cutaneous cues for softness estimation. However, cutaneous cues play a major role in softness perception. Both these cues also took part in participants' curvature perception. When participant touch and explore curved surfaces with different softness, both types of cues can vary based on curvature *and* softness. E.g., both the cutaneous cues of pressure distribution around the contact area and the kinesthetic cues of finger position can be different because of the different surface deformation and/or finger pad deformation. Consequently, there might be an impact of softness on curvature perception. For this reason, we study here the impact of softness on curvature perception.

3 EXPERIMENT

The goal of our experiment is to explore whether the softness impacts participants' ability to discriminate between different surface curvatures. For this, we use a method called *constant stimuli* [70, 71, 86]. This method presents successively to participants two stimuli in a random order in a trial: one with the reference curvature as the stimulus of reference, and another with a different curvature as the stimulus of comparison (Figure 2(a) top right). It then assesses if they can discriminate the most curved stimulus. This enables us to measure the just noticeable difference (JND) and the point of subjective equality (PSE) in curvature discrimination with stimuli of different softness. We also measure the exploration time participants needed for discrimination.

3.1 Experimental parameters

Our independant variables were SOFTNESS and CURVATURE:
SOFTNESS: *Shore 00-10*, *Shore 00-50*, *Shore A-30* and *Rigid* (bottom of Figure 1). The rigid stimuli served as a baseline and to compare our results to prior work [70]. As users categorize an object as hard or soft based on whether the object is more or less soft than the finger pad [25], we chose the experimental levels of softness based on existing measurements of the index finger pad hardness ($\approx$ Shore 00-50) [17, 19]. The softness of our soft stimuli was designed to be (1) softer (Shore 00-10), (2) as soft as (Shore 00-50), and (3) harder (Shore A-30 $\approx$ Shore 00-80 [57]) than the index finger pad.
CURVATURE: To investigate perceptual sensitivity over a broad range of UI curvatures, we studied 3 different curvatures levels: *very curved*, *middle curved*, and *little curved* as in [70]. Each curvature condition corresponds to a stimulus of reference with radius R_{ref}=10, 20 and 40 mm. Participants were presented with 6 stimuli whose curvature clustered around the comparative stimulus of reference as in [70]:

(a) A participant exploring our stimuli. The first stimulus exits following the direction of the red arrow and the second stimulus enters following the blue arrow.

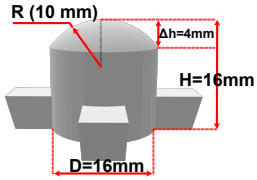

(b) R indicates the radius of the curved surface. The smaller the radius means the more curved the surface. Δh indicates height change over the curved surface ($\Delta h = R - \sqrt{R^2 - D^2/4}$).

(c) Example stimuli: the left one is the most curved (R = 8.3 mm), and the right one is the flattest (R = 52.6 mm)

(d) (Left) The pressure sensor Interlink FSR406 stuck on the 3D printed support and (middle) a stimulus to install on this support. (Right) The schematics of the circuit for one sensor.

Figure 2: (a) Experimental setup, (b) 3D model of a very curved stimulus, (c) photograph of two stimuli (from the group of softness Shore 00-50) used in our experiment, and (d) pressure sensor and schematics of the circuit for sensor reading (as in [27]).

- Very curved (R_{ref}=10 mm): R=8.3, 8.8, 9.4, 10.7, 11.5 and 12.5 mm;
- Middle curved (R_{ref}=20 mm): R=16.7, 17.6, 18.8, 21.4, 23.1 and 25 mm;
- Little curved (R_{ref}=40 mm): R=32.3, 34.5, 37, 43.5, 47.6 and 52.6 mm.

In each curvature condition, three stimuli of comparison were more curved than the reference stimulus, three were less curved than the reference stimulus, and their curvatures (in m^{-1}) were equally spaced, as explained in [30]. Figure 2(c) shows one stimulus with the most curved surface (R=8.3 mm) and one with the flattest surface (R=52.6 mm) from the group of softness Shore 00-50.

3.2 Participants

We recruited 12 participants (6 women, 6 men, M=26.1 years old, SD=4.1 years) at the local university. One participant was left-handed. Each participant received a voucher worth 50€. We measured the hardness of participants' dominant index finger pad with a BAREISS HP Shore 00 durometer. The measurement followed a standard procedure [19]. The average hardness of participants' finger was Shore 00-38.28 (SD=Shore 00-4.43).

3.3 Stimuli

We used 84 stimuli in total: 4 SOFTNESS × 3 CURVATURES levels × 7 stimuli (6 comparison stimuli + 1 reference stimulus). We printed the rigid stimuli with photo-polymer resin (Formlabs standard clear resin) using a stereo-lithography 3d printer (Formlabs Form3). We fabricated the molds for the soft stimuli with the same printer and with the same resin as the one used for the rigid stimuli. We used three types of silicone from *Smooth-On, Inc.* for our soft stimuli: Ecoflex 00-10, Ecoflex 00-50, and Dragon Skin 30 respectively for softness levels Shore 00-10, Shore 00-50, and Shore A-30. We followed instructions from *Smooth-On, Inc.* for molding and unmolding. We verified the actual curvatures of the fabricated stimuli as in [79] and report them in appendix B.

All our stimuli had the same height and the same base diameters. This prevents confounding haptic cues from height [69] and contact area [35]. We chose for our stimuli a base-to-peak height of 16 mm and a diameter of 16 mm, as shown in Figure 2(b). The width (i.e., diameter) of our stimuli is similar to the a human's index finger pad [12] and to many existing soft UIs (e.g., [4, 24, 93]). The height of our stimuli allows participants to freely rest their arms and wrists on the table to avoid fatigue during the experiment and is similar to the height used in [55]. The 3D models of the stimuli or their molds are provided in the supplementary material for replication.

We used magnesium powder to reduce friction between the skin and the silicone surface as in [37]. We spread the magnesium powder evenly over all stimuli with a chalk ball before each experimental session. During the experiment, participants can freely access the chalk ball to spread the magnesium powder on their fingers when feeling too much friction.

3.4 Experimental setup and procedure

Participants first signed an informed consent form and filled out a short demographic questionnaire. As shown in Figure 2(a), participants sat at a table while their arms and wrists rested freely on the table to avoid fatigue during the experiment. They freely explored the curvature of the stimuli with the index finger of their dominant hand. A box prevented participants from seeing their fingers and the stimuli. In front of the participants, we installed a camera on a tripod to record participants' finger movements when exploring our stimuli (Figure 2(a)).

Our experiment used a two-alternative forced-choice procedure. In each trial, we presented the pair of stimuli to compare sequentially, as we are interested to know if users can perceive a change

Figure 3: Experimental procedure with the first repetition illustrated: this participant first experienced the middle curvature (R_{ref}= 20 mm). Every pair in the illustrated repetition indicates the radii of the curved surfaces successively presented in one trial. In every pair, one of the radii is of the reference stimulus (R_{ref}=20 mm).

in the curvature of a single "widget" –such as a button changing its curvature over time– as many interactive devices do, e.g., [32, 40, 91]. We chose to have an interruption, as small as possible, between the exploration of each stimulus, as this is the most common procedure [51] and users sometimes take their finger off the UI in real situations. We expect this method to measure a safer JND for designers as prior work showed that continuous exploration of both stimuli –i.e. with no interruption in the exploration of both comparison stimuli– resulted in a smaller JND in compliance [51].

We aim at a quick switch between the two stimuli to be compared, to decrease the "time error" due to the memory of the first stimuli fading with time [51, 70]. For this, as shown in Figure 2(a), the experimenter places both stimuli to be compared on a 3D printed rail guide. When switching, the support guides the sliding of the first stimulus out of the participant's reach, and the sliding of the second stimulus precisely below the participant's finger. The average switching time between two stimuli in our experiment was 2.25 s (SD= 0.21 s), similarly to prior work [34, 35, 71].

A participant had to indicate which of the two presented stimuli (Figure 2(a) top right) felt more curved (as in [88]) by saying "first" or "second". No restrictions were imposed on the exploration time of each stimulus, as in [71, 88, 89].

As the example shown in Figure 2(d) (left), we stuck a 39.6×39.6 mm^2 commercial pressure sensor (*Interlink FSR406*[3]) on each 3D printed support with double-sided tape. This sensor enables the recording of the force that participants applied to our stimuli when exploring our stimuli. Figure 2(d) (right) shows the schematics of the trans-impedance circuit that we implemented to ensure a nearly linear output of our sensors, following the guide of the vendor (Interlink Electronics) similar to the circuit implemented in [27]. We used a *Teensy2* to read the sensors' output.

We developed a software running on macOS using PyQT5 for the experimenter to quickly and correctly present the stimuli, and to record the exploration time and the exploring force of each stimulus, and the participants' answers. The exploration time of the first stimulus was defined as the duration between the time when the experimenter asked the participants to start exploring the first stimulus, and the time participants signaled the experimenter that they completed their exploration. Then the experimenter switched the stimuli as presented in Figure 2(a) and asked participants to explore the second one. The exploration time of the second stimulus was defined as the duration between the time when the experimenter asked the participants to start exploring the second stimulus, and the time participants answered "first" or "second" as the most curved.

[3]https://www.interlinkelectronics.com/fsr-406

3.5 Experimental design

Independent variables were SOFTNESS and CURVATURE. We used a fully-crossed, within-subjects factorial design with repeated measures. Every participant experimented with all softness and curvature conditions.

The first dependent variable was the percentage of times the participants responded that the stimulus of comparison felt more curved than the stimulus of reference. The second dependent variable was the exploration time, for both first and second exploration of a trial of discrimination between two stimuli.

As shown in Figure 3, we had in total 3 series of experimental comparisons, one for each curvature level. Participants trained before each series. For this, they compared the two most different pairs of stimuli, i.e., the least and the most curved to the current reference stimulus. The softness of the training stimuli was chosen randomly. As in [69], the experimenter gave feedback on the correctness of the answer during the training, and the experimental series started after participants correctly judged four of these combinations successively. In each series, we had four blocks of experimental comparisons, one block for each softness condition. Each block was repeated three times. In each block of experimental comparisons, we repeated twice each of the 6 possible comparisons to the reference stimulus, in opposite order [70]. This lead to 12 trials per block. Figure 3 shows an example of 12 trials that one participant experienced. As in [88], the participants did not know that the reference stimulus was presented in all trials. As in [69, 88], participants did not receive feedback on their performance during the experiment.

After finishing all 12 trials of one block, participants were allowed to take a short break until they felt ready for the next block. The order of presentation of the three series was randomized. The order of presentation of the four blocks was counterbalanced across participants according to a Latin square. The order of presentation of 12 trials in one block was pseudo-randomized. Each series of experimental comparisons took around 75min. Participants completed each series of experimental comparisons on three different half-days to reduce the impact of fatigue. After each series, participants filled a short 5 items Likert-scale questionnaire to evaluate the difficulty of the curvature discrimination in each softness condition from very easy to very difficult. In total, the experiment took 4 hours for each participants.

Following previous work, we draw the following three hypotheses for all curvature conditions:

H1: The softer the surface, the lower participants' curvature perception precision, i.e., the larger the just noticeable difference (JND) in curvature.

H2: The softer the surface, the lower the participants' curvature perception accuracy, i.e., the larger distance between the point of subjective equality (PSE) and the reference curvature.

H3: The softer the surface, the slower participants discriminate the curvature, i.e., they take longer exploration time for the first stimulus, for the second stimulus, and for their average.

In order to reduce unintentional false positive inflation of results [95], our study was registered before collecting the data[4].

4 DATA PRE-PROCESSING AND ANALYSIS

4.1 Just-noticeable difference (JND) and Point of subjective equality (PSE)

We computed the JND and PSE values for each participant in each softness × curvature as in [59]. We first fit the proportion of times participants reported the comparison stimulus as the least curved with a Generalized Linear Model using a probit link function [59] to obtain a psychometric curve based on standard psychophysical protocol [30, 59]. Figure 4(a) presents an example of a psychometric curve, resulting from the fitting of participant P2's responses when discriminated stimuli with R_{ref}=10mm and SOFTNESS=Shore 00-50.

We then estimate the PSE and JND values based on the psychometric curve obtained with the fit functions based on standard psychophysical protocol [30, 59]. The PSE refers to the 50% point on the psychometric curve, where participants have half chance on average to judge the comparison reference less curved than the reference stimulus (e.g., 10.2 mm in Figure 4(a)). The PSE is a measure of participants' perception accuracy [59]. A PSE closer to the reference curvature (e.g., closer to 10 mm in Figure 4(a)) means less perception bias, thus better accuracy.

The distance between the 50% point and 75% point on the psychometric curve (e.g., 10.7 mm in Figure 4(a)) indicates the JND (e.g., 0.5 mm in Figure 4(a)). The JND indicates the threshold of difference in curvature that can be perceived with a probability halfway between a chance response (i.e., 50%) and an always-correct response (i.e., 100%). The JND refers to participants' perception precision: the smaller the JND, the better the precision [59].

4.2 Analysis

We use estimation techniques based on means and 95% bootstrapped confidence intervals (CI) as recommended by Dragicevic [15], and pairwise differences to show effect sizes. These methods are recommended by the APA [2] and largely adopted [13, 14, 44, 48, 53, 62]. We opted for this nuanced analysis of the direction and magnitude of the effect. A pairwise difference is an intra-subject measurement that expresses the effect size and is computed between each mean. This allows to quantify the difference per participant.

For readers expecting dichotomous inference, we additionally present an analysis based on p-value. A Shapiro-Wilk test showed that we could not assume the normality of our data. Therefore, we performed an aligned rank transformation [94] of the data before a repeated measure ANOVA. As we study the perception of curvature for soft devices that used curvature to provide feedback, we analysed the impact of softness on each curvature condition (i.e., each R_{ref}) independently. We did not analyse the interaction between SOFTNESS and CURVATURE. For post-hoc tests, we used Wilcoxon Signed-rank tests using Holm's sequential Bonferroni procedure for p-value correction. Detailed results of post-hoc tests can be found in appendix A. The analysis software and detailed results are available as supplementary material.

[4]Registration of the experiment available at http://osf.io/scnj9/

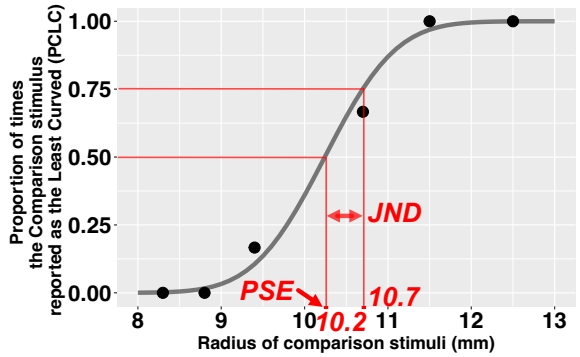

(a) Proportion of times P2 reported the comparison stimulus as less curved than the reference stimulus for *Shore 00-50* and R_{ref}=10 mm and its psychometric function fit.

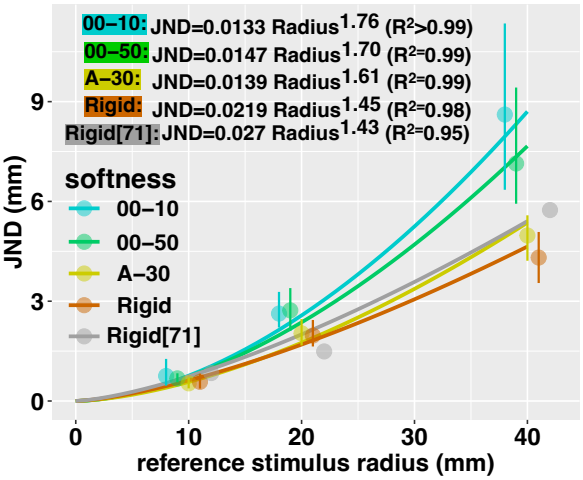

(b) JND results for all CURVATURES and SOFTNESS. The results were fitted by a power curve [71, 82]. Data points were slightly jittered horizontally to avoid overlap. The gray color shows Provancher et al.'s data [71].

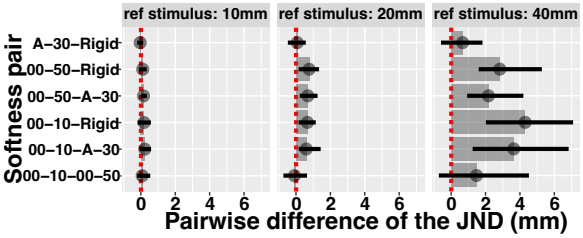

(c) JND pairwise differences between each softness pair (Y axis) for each curvature condition, computed for each participant individually and averaged.

Figure 4: Just noticeable difference computation and results.

5 RESULTS

5.1 Just noticeable difference (JND)

H1 is partially verified: Participants do not have a lower curvature perception precision with a softer surface. I.e., not in all curvature condition, they had a larger JND of curvature in a softer condition.

Figure 4(b) shows that **in the most curved condition (R_{ref}=10 mm), participants performed with similar perception precision in all four softness conditions** : Shore 00-10 JND= 0.75 mm (CI [0.45, 1.25]), Shore 00-50 JND= 0.68 mm (CI [0.56, 0.83]), Shore A-30 JND= 0.53 mm (CI= [0.38, 0.71]), Rigid JND= 0.58 mm(CI= [0.38, 0.83]). We did not measure an effect of softness. It is consistent with the pairwise difference shown in Figure 4(c): the error bars of all softness pairs cross zero in CURVATURE=10 mm condition. Consistently, ANOVA also shows no significant impact of softness on curvature perception precision ($F_{(3,33)}$=0.63, p=0.6) in this curvature condition.

In middle curved condition (R_{ref}=20 mm), participants performed with similar perception precision in the two softest conditions: Shore 00-10 JND=2.63 mm (CI [2.20, 3.28]), Shore 00-50 JND= 2.72 mm (CI [2.09, 3.38]). **Participants also performed with similar perception precision in the two hardest conditions**: Shore A-30 JND=2.03 mm (CI [1.67, 2.46]), Rigid JND=1.97 mm (CI= [1.64, 2.44]). **Participants performed with better perception precision in the two hardest conditions than in the two softest conditions.** ANOVA also shows the significant impact of softness on curvature perception precision ($F_{(3,33)}$=2.94, p<0.05) in this curvature condition. It is consistent with the pairwise differences shown in Figure 4(c): in R_{ref}=20 mm condition, only the error bars of the pairs *Shore 00-10–Shore 00-50* and *Shore A-30–Rigid* cross zero. However, post-hoc tests show no significant difference between any softness pairs (Table 2 in appendix A). This can result from a small difference (see Figure 4(b)). What we learn from this experiment is that the curvier, the less the impact of the softness of the curvature perception. R_{ref}=20 mm might lie at the limit of curvature where this happens.

In the flattest condition (R_{ref}= 40 mm), participants performed with better precision in the more rigid conditions (Figure 4(b)): Shore 00-10 JND=8.61 mm (CI [6.35,11.36]), Shore 00-50 JND=7.14 mm (CI [5.93,9.38]), Shore A-30 JND=4.93 mm (CI [4.24,5.58]), Rigid JND=4.32 mm (CI [3.53,5.06]). ANOVA consistently shows the significant impact of softness on curvature perception precision in this curvature condition ($F_{(3,33)}$=4.9, p<0.01). However, in Figure 4(c), in R_{ref}=40 mm condition, the error bars of the pairs of *Shore 00-10–Shore 00-50* and *Shore A-30–Rigid* cross zero. This suggests **similar perception precision in the two hardest conditions and also in the two softest conditions, for the flattest curvature. Participants performed with better perception precision in the two hardest conditions than in the two softest conditions.** Post-hoc tests (Table 2) confirms the significant difference between the softness pairs of *Shore 00-10–Rigid*, *Shore 00-50–Rigid*, *Shore 00-50–Shore A-30*, but not between the other softness pairs. These might be explained by a higher variability among participants, because the error bars are larger in R_{ref}=40mm in Figures 4(b) and 4(c).

Figure 4(b) shows that participants' JND increased as the stimuli become flatter from R_{ref}=10 mm to 40mm. More precisely, the power-law fit results in Figure 4(b) show that the exponent increases from 1.45 to 1.76 as the stimuli become softer from Rigid to Shore 00-10. In addition, all exponents are larger than 1. This suggests that, with a softer material, participants' curvature perception precision may more strongly decrease as the surface becomes flat. In addition, the difference in perception precision between different softness conditions may be larger as the surface becomes flat.

Interestingly, Provancher et al. conducted similar curvature perception experiments with only rigid stimuli [70, 71]. Their results are shown in gray on Figure 4(b). Their results are similar to our result with the rigid condition, with a slightly lower JND with R_{ref}=20 mm and a slightly higher JND with R_{ref}=40 mm. We further discuss our replication of their experiment with rigid stimuli in section 6.1.

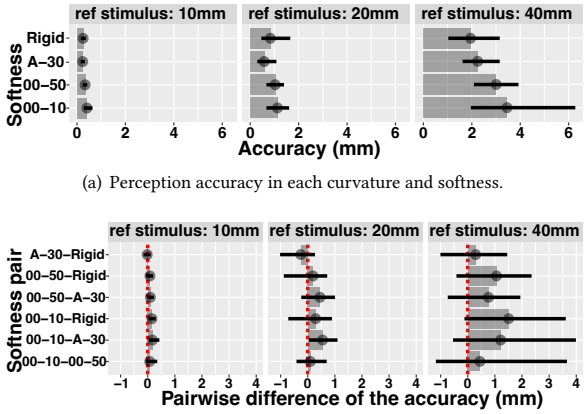

(a) Perception accuracy in each curvature and softness.

(b) Pairwise difference in accuracy between pairs of softness.

Figure 5: Accuracy (i.e. distance between PSE and reference curvature).

5.2 Point of Subjective Equality (PSE)

H2 is not verified: Participants do not have a lower curvature perception accuracy with a softer surface. I.e., there was not a larger distance between the PSE and the reference curvature in softer conditions in each curvature condition.

Figure 5(a) shows that participants tended to be less accurate when exploring less curved surfaces. The average distance between PSE and the reference curvature is 0.31 mm (CI=[0.26,0.38]) for R_{ref}=10mm, 0.90 mm (CI=[0.69,1.15]) for R_{ref}=20mm, and 2.67 mm (CI=[2.12,3.48]) for R_{ref}=40mm. **In the most curved condition (R_{ref}=10 mm), participants performed with similar perception accuracy in all four softness conditions**. The distance between the PSE and the reference curvature is 0.41 mm (CI [0.29, 0.63]) for Shore 00-10, 0.34 mm (CI [0.24, 0.43]) for Shore 00-50, 0.24 mm (CI [0.15, 0.33]) for Shore A-30, and 0.25 mm (CI [0.16, 0.37]) for rigid. We did not measure an effect of softness. It is consistent with the pairwise differences shown in Figure 5(b): the error bars of all softness pairs cross zero when R_{ref}=10 mm.

In the middle curved condition (R_{ref}= 20 mm), participant performed with the highest perception accuracy in the little rigid condition and the lowest perception accuracy in the softest condition. The distance between the PSE and the reference

curvature is 0.58 mm (CI [0.29, 1.09]) in the Shore A-30 condition, and 1.13 mm (CI [0.67, 1.62]) in the Shore 00-10 condition. Participants' perception accuracy with Shore 00-50 and Rigid conditions were similar and located between the accuracy of the previous other two softness conditions. The distance between the PSE and the reference curvature is 1.03 mm (CI [0.67, 1.41]) with Shore 00-50 and 0.83 mm (CI [0.45, 1.65]) with rigid stimuli. All error bars in R_{ref}=20 mm condition (Figure 5(b) cross zero or near it. This suggests that **participants' perception accuracy was similar in all four softness conditions.**

In the flattest condition (R_{ref}=40 mm), participants performed with decreasing perception accuracy with softer conditions (Figure 5(a)). The distance between the PSE and the reference curvature is 3.46 mm (CI [1.96, 6.29]) with Shore 00-10, 3.01 mm (CI [2.08, 3.93]) with Shore 00-50, 2.24 mm (CI [1.62, 3.14]) with Shore A-30, and 1.95 mm (CI [1.04, 3.14]) with rigid stimuli. However, Figure 5(b) shows that error bars of the pairwise comparisons between all six softness pairs cross zero for R_{ref}=40 mm. This suggests that participants had **similar perception accuracy in all four softness conditions with the flattest curvature.**

ANOVA shows consistent results. In all three curvature conditions, the softness has no significant impact on the curvature perception accuracy (R_{ref}=10 mm: $F_{(3,33)}$=1.59, p=0.21; R_{ref}=20 mm: $F_{(3,33)}$=1.42, p=0.25; R_{ref}=40 mm: $F_{(3,33)}$=1.17, p=0.34).

5.3 Exploration time

H3 is partially verified: Participants do not discriminate curvature slower with a softer surface. I.e., not in all curvature conditions, participants needed longer exploration time for the first stimulus, for the second stimulus, and for their average in softer conditions.

Figure 6(a) shows that participants need much less time to explore the second stimulus in a trial after completing the exploration of the first one. This applies to all reference curvature and softness conditions. After taking the time to memorize the first stimulus, participants make their decision faster with the second stimulus.

In all three curvature conditions, the softer the stimulus, the longer the exploration times (Figure 6(a)). For instance, when R_{ref}= 10 mm, participants' average exploration time increased from 3.21 s (CI [2.70, 4.03]) when exploring the rigid stimuli to 3.46 s (CI [2.85, 4.37]) when exploring the softest stimuli (Shore 00-10). When R_{ref}= 20 mm, participants' average exploration time increased from 3.54 s (CI [2.87, 4.64]) to 4.04 s (CI [3.17, 5.24]). When R_{ref}= 40 mm, participants' average exploration time increased from 3.98 s (CI [3.11, 5.57]) to 4.37 s (CI [3.42, 5.78]). However, there are large overlaps of error bars in almost all three curvature conditions for all the three exploration times. This indicates the **slow increase of the necessary time to explore the curvatures of softer surfaces.** This is consistent with the pairwise differences of exploration times (Figure 6(b)). Seven out of the nine *Shore 00-10–Rigid* pairwise comparisons do not cross zero, showing that there is a major increase of exploration times between the softest and the rigid condition. However, all the error bars of the pairwise difference of exploration time of two neighbor softness pairs cross zero or near it (*Shore 00-10–Shore 00-50*, *Shore 00-50–Shore A-30*, *Shore A-30–Rigid*). The only exception is the pairwise difference of exploration time of *Shore 00-10–Shore 00-50* for R_{ref}=40mm. In these conditions,

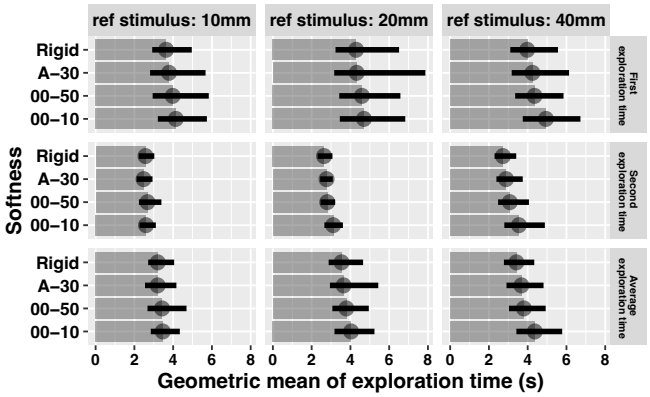

(a) Exploration time of the first stimulus of a trial (top), of the second stimulus (middle), and their average (bottom), in each curvature and softness condition.

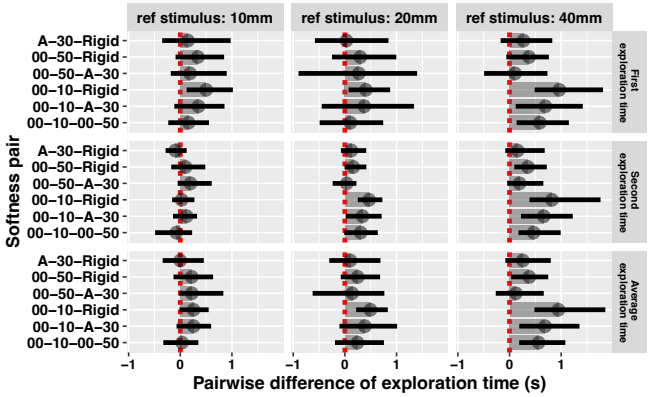

(b) Pairwise difference of the time between pairs of softness for each curvature condition.

Figure 6: Exploration time.

the pairwise difference of exploration time is 0.59 s (CI [0.14, 1.15]) for first stimulus, 0.47 s (CI [0.17, 0.99]) for the second stimulus, and 0.56 s (CI [0.18, 1.08]) for their average. This exception suggests that **in the flattest condition (R_{ref}=40 mm), participants need a much longer exploration time (all for the first stimulus, the second stimulus, and their average) when exploring the softest (Shore 00-10) stimuli than other softness conditions** including its neighbor softness condition (Shore 00-50).

ANOVA shows that in the two curviest conditions (R_{ref}= 10 and 20 mm), the impact of softness on the exploration time is not significant, neither for the first stimulus, nor for the second stimulus, nor for their average in softer conditions (R_{ref}= 10 mm: $F_{(3,33)}$=2.03, p=0.13; $F_{(3,33)}$=0.61, p=0.61; $F_{(3,33)}$=1.23, p=0.31. R_{ref}= 20 mm: $F_{(3,33)}$=1.24, p=0.31; $F_{(3,33)}$=2.44, p=0.08; $F_{(3,33)}$=1.44, p=0.25).

In the flattest condition (R_{ref}=40 mm), ANOVA shows a significant impact of softness on the exploration time, both for the second stimulus and for their average in softer conditions ($F_{(3,33)}$ = 4.38, p<0.05; $F_{(3,33)}$ = 4.44, p<0.01), but not for the first stimulus ($F_{(3,33)}$ = 2.59, p=0.07). Post-hoc tests confirms the significant difference in exploration time between the softest condition (Shore 00-10) and the rigid condition (Table 3 in appendix A).

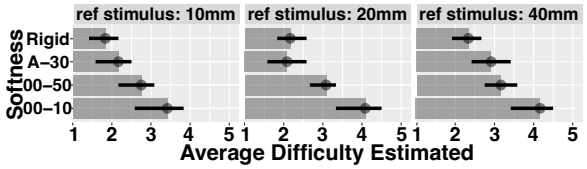

(a) The curvature perception difficulty estimated by participants in each curvature and softness condition, from 1 (very easy) to 5 (very difficult).

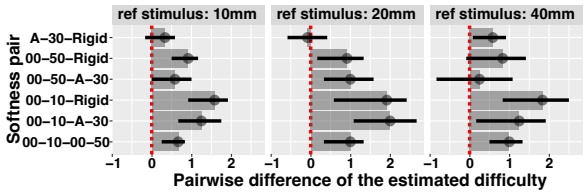

(b) Pairwise difference in subjective difficulty between two softness for each curvature condition.

Figure 7: Subjective discrimination difficulty.

5.4 Difficulty estimation

In addition to the three measures registered[4], i.e., JND, PSE, and Exploration time, we also studied participants' subjective difficulty to discriminate the curvatures. Figure 7(a) shows that **participants clearly found more difficult to discriminate between curvatures when the material is softer.** E.g. in the most curved condition (R_{ref}=10 mm), participants found it rather easy (M=1.83, CI [1.42, 2.17]) to discriminate the rigid stimuli. However, they found it rather neutral (M=3.42, CI [2.58, 3.83]) to discriminate the softest stimuli. In the middle curved condition (R_{ref}=20 mm), participants found it rather easy (M=2.17, CI [1.83, 2.59]) to discriminate the rigid stimuli. However, they found it rather difficult (M=4.08, CI [3.33, 4.50]) to discriminate the softest stimuli. In the little curved condition (R_{ref}= 40 mm), participants found it rather easy (M=2.33, CI [1.92, 2.75]) to discriminate the rigid stimuli. However, they found it rather difficult (M=4.17, CI [3.42, 4.50]) to discriminate the softest stimuli. These results are consistent with the pairwise differences shown in Figure 7(b). All the error bars of the pairwise differences between Shore 00-10 and rigid do not cross zero.

ANOVA also shows the significant impact of softness on participants' subjective difficulty to discriminate the curvatures in all three curvature conditions (R_{ref}=10 mm: $F_{(3,33)}$ = 16.96, p<0.001; R_{ref}=20 mm: $F_{(3,33)}$ = 14.84, p<0.001; R_{ref}=40 mm: $F_{(3,33)}$ = 8.48, p<0.001). Post-hoc tests confirm that in all three curvature conditions, participants estimated that discrimination of the curvature with the softest stimuli (Shore 00-10) is significantly more difficult than with all three other softness, except the Shore A-30 stimuli when R_{ref}=40 mm (Table 2 in appendix A).

6 DISCUSSION

6.1 Partial replication of prior work

Our experiment, through the curvature perception of rigid curved surfaces, was a partial replication of previous work [70, 71]. While we shared the same curvature levels of stimuli used in prior work, we extended the scope of Provancher et al.'s experiment to stimuli with different softness. In their experiment, participants rolled their index finger along the circumferential direction of rigid cylinders with different radii to explore their curvature. On the contrary to our stimuli that had spherical surfaces, Provancher et al.'s stimuli were curved only in the direction along the finger (distal-proximal direction), not in the direction across the finger (radial-ulnar direction). The reason for this difference is that one of our objectives was to prepare guidelines for the design of soft curvature-changing UIs, such as buttons [32, 40, 91]. We found that spherical shapes were more widespread than cylindrical shapes in soft curvature-changing UIs. For instance, Pneumatibles [32], Fingertip Softness Tactile display [24], Haptic Jamming [81], and Inflatable Hemispherical Multi-touch Display [83] are soft curvature-changing UIs with spherical shapes.

Another difference with their experiment is the diameter D of the stimuli base cylinder (Figure 2(b)). In their experiment, the flatter the stimulus (i.e., the larger the radius of the curved surface), the larger the diameter of the stimulus. In our experiment, as shown in Figure 2(b), all of our stimuli had the same base diameter. A reason for this difference is that we wanted to prevent any confounding cues from the contact area [35], because a larger diameter can result in a larger contact area with the participants' finger pads, in addition to larger exploratory movements. Another reason for this difference is that one of our objectives was to prepare guidelines for the design of soft curvature-changing UIs. Curvature and size are two independant dimensions of shape-changing UIs [49], and curvature-changing UIs do not necessarily change their size (e.g., [32]). In addition, enlarging a UI might be troublesome because of geometrical constrains from the body or environment [1]. Future work should study the impact of the base diameter.

As shown in Figure 4(b), Provancher et al. curvature perception precision (i.e., JND) of rigid surfaces was similar to ours in R_{ref}=10 mm: 0.84 mm [71] vs. 0.58 mm (CI [0.38, 0.83]). For R_{ref}=20 mm, Provancher et al.'s participants were slightly more precise: 1.49 mm [71] vs. 1.97 mm (CI [1.64, 2.44]). For R_{ref}=40 mm, Provancher et al.'s participants were slightly less precise: 5.74 mm [71] vs. 4.31 mm (CI [3.53, 5.06]).

We hypothesize that these differences come from the two types of cues in curvature perception: the kinesthetic and cutaneous cues. Pont et al. [69] found that kinesthetic cues were effective for participants to discriminate surface curvature. In particular, when users slide their finger over the stimulus to explore the curvature, an effective cue is the total height change over the surface. In other words, users discriminate from the the ratio between the height and width of stimuli, i.e. the ratio of $\frac{\Delta h}{D}$ in Figure 2(b). As a consequence, when two stimuli have the same curvature but are of different base diameters, the larger stimulus has the larger total height change over the surface ($\frac{\Delta h}{D}$), and therefore, this can improve participants' curvature perception precision. When R_{ref}=20 mm, the base diameter of Provancher et al.' cylindrical stimuli was larger than ours (see Figure 4-6 in [70]). For this reason, their participants could get stronger kinesthetic cues from rolling their fingers on the stimuli than our participants. This might explain why they found better precision when R_{ref}=20 mm. However, this cannot not explain why Provancher et al.'s curvature JND was slightly less precise when R_{ref}=40 mm.

Vogels et al. studied participants' curvature discrimination absolute threshold, i.e., the just noticeable difference between a curved surface and a flat surface ($0m^{-1}$), through static touch –which involves only cutaneous cues. They studied stimuli with double curved surfaces (e.g., spherical and elliptical). They found a lower threshold ($0.2 - 0.32m^{-1}$, i.e., corresponding radius $3.125 - 5m$) than the threshold found by Pont et al. in [68] ($0.5 - 0.9m^{-1}$, i.e., corresponding radius $1.11 - 2m$) with cylindrical stimuli. This suggests that double curved surfaces (e.g., spherical surfaces) could provide participants with better cutaneous cues than single curved surfaces (e.g., cylindrical surfaces). In our experiment, participants touched and explored stimuli with spherical surfaces, which should provide them with better cutaneous cues than stimuli with cylindrical surfaces [70, 71]. When exploring stimuli in R_{ref}=40 mm, the kinesthetic cue weakened both in Provancher et al.'s and our experiment because of smaller ratio of $\frac{\Delta h}{D}$ (detailed calculation in supplementary material). The cutaneous cues might play an more important role in curvature discrimination, while the kinesthetic cue was weaker. This might explain why the precision we found when R_{ref}=40 mm was better than prior work [70, 71].

We suppose that in nearly flat condition, the kinesthetic cues were so weak that the cutaneous cues played a more important role, while kinesthetic played a more important role when the surface curvatures were more curved (R_{ref}=20 mm). When exploring surfaces very curved (R_{ref}=10 mm), we suppose that both cutaneous and kinesthetic cues were strong, and participants can well combine them. Thus, if one of these cues is weaker, participants' perception precision should not significantly decrease. This may also explain why users had similar perception precision and accuracy with very curved surfaces in different softness conditions.

6.2 Impact of softness on precision (JND)

To propose an explanation of the impact of softness on JND as the surface becomes flatter, we use Hertz contact theory [45]. Hertz contact theory provides a model for the contact between two elastic bodies. Even though Hertz contact theory is a rough model of finger pad contact [64], it helps to understand the process when our finger touches soft curved surfaces. Based on Hertz contact theory, we can roughly simplify the contact and deformation between participants' finger pads and our curved surfaces as the contact and deformation between two elastic curved spheres [6, 75] with respectively the radius of $R_{FingerPad}$ and $R_{Stimulus}$, and Young's modulus of $E_{FingerPad}$ and $E_{Stimulus}$. The contact area between a finger and a curved soft stimulus can be approximated as a circle with the following radius r [6, 75]:

$$r = \left(\frac{3PR}{4E}\right)^{\frac{1}{3}} \tag{1}$$

Where P is the pressure that participants applied to the stimulus, R is the the relative radius of curvature, and E is the equivalent modulus. These variables depend on the radius and Young's modulus of participants' finger pad [64] and the stimulus: $E = \left(0.75\left(\frac{1}{E_{Stimulus}} + \frac{1}{E_{FingerPad}}\right)\right)^{-1}$ and $R = \left(\frac{1}{R_{Stimulus}} + \frac{1}{R_{FingerPad}}\right)^{-1}$.

To simplify the analysis of the impact of the stimulus curvature $R_{Stimulus}$ and stimulus softness $E_{Stimulus}$ on the deformation, we suppose that:

$$E_{FingerPad} = a\ E_{Stimulus}, \quad R_{FingerPad} = b\ R_{Stimulus} \tag{2}$$

Where a and b are participant-dependent constants. Then, the relative radius of curvature R and the equivalent modulus E can be written as: $E = \frac{4a}{3(a+1)}\ E_{Stimulus}$, $R = \frac{b}{b+1}\ R_{Stimulus}$. Equation 1 can then be simplified as $r = \left(\frac{9b(a+1)}{16a(b+1)}\right)^{\frac{1}{3}}\left(\frac{PR_{Stimulus}}{E_{Stimulus}}\right)^{\frac{1}{3}}$. As $\left(\frac{9b(a+1)}{16a(b+1)}\right)^{\frac{1}{3}}$ is constant for each participant, we can set it as a constant C in the purpose of simplifying the analyze. Equation 1 can then be simplified as:

$$r = C\left(\frac{PR_{Stimulus}}{E_{Stimulus}}\right)^{\frac{1}{3}} \tag{3}$$

According to equation 3, either the increase of stimulus softness (i.e., smaller $E_{Stimulus}$) or the decrease of stimulus curvature (i.e., larger $R_{Stimulus}$) will lead to a larger contact area.

The JND power-law fit on Figure 4(b) shows that the softer the stimuli, the larger the exponent. In addition, all exponents were larger than 1. This suggests that, with a softer material, participants' curvature perception precision may more strongly decrease as the surface becomes flat. Also, the difference in perception precision between different softness conditions may be larger as the surface becomes flat. To better understand the impact of surface softness on contact area under different curvature conditions, we can calculate the derivatives of r over $E_{Stimulus}$:

$$\frac{\partial r}{\partial E_{Stimulus}} = -\frac{C}{3}\left(PR_{Stimulus}\right)^{\frac{1}{3}} {E_{Stimulus}}^{-\frac{4}{3}} \tag{4}$$

According to equation 4, with flatter stimuli (i.e., larger $R_{Stimulus}$), the contact area increases more rapidly with softer stimuli (i.e., smaller $E_{Stimulus}$). This is consistent with our JND power-law fit result: Figure 4(b) suggests a larger difference in perception precision between different softness conditions as the surface becomes flatter. This might be explained by the surface and/or the finger pad deformation. On the one hand, a larger contact area slightly improves participants' perception precision [35] when passively touching rigid stimuli. On the other hand, the larger contact area means also bigger deformation of the stimulus and the finger pad. This deformation might inversely harm our perception of the shape, e.g., when stimuli are too flat and/or too soft. So far, this did not explain why participants could perform in soft conditions as precisely as in rigid conditions with our most curved stimuli (R_{ref} =10 mm). We suppose the reason is that both cutaneous and kinesthetic cues were strong enough. A slight deformation of the stimulus and/or the finger pad should then not significantly decrease participants' precision.

6.3 Similar accuracy with different softness

One of our main finding was that participants' perception accuracy did not differ systematically between different softness conditions in all curvature conditions. Yet, when exploring less curved surfaces, participants tended to be less accurate.

Previous work found factors possibly biasing participants' curvature perception accuracy with *rigid* stimuli. Among them, Vogels et al. [92] observed bias from the shape of the surface around participants' fingers: they experimented with stimuli with double curved

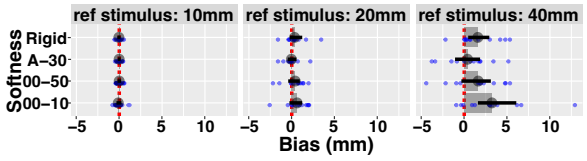

(a) Perception bias in each CURVATURE and SOFTNESS.

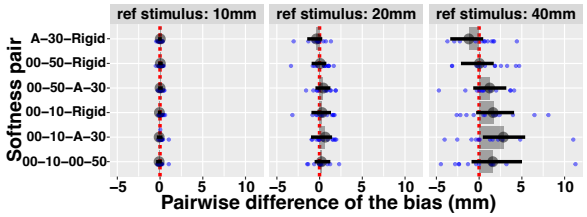

(b) Pairwise difference in bias between two SOFTNESS for each CURVATURE.

Figure 8: Perception bias (i.e., signed difference PSE - R_{ref}).

surfaces (e.g., spherical and elliptical), which can be defined by two principal curvatures. They found that the curvature in the direction perpendicular to participants' finger (radial–ulnar direction) biases participants' perception accuracy of the curvature along their finger (distal-proximal direction). E.g., their participant judged a curvature to be more convex when the perpendicular curvature was convex than when this curvature was concave. The fact that participants tended to be less accurate (i.e., larger absolute values bias) when exploring less curved surfaces in our experiment might be explained by the bias of the shape of the surface around participants' fingers [92]. The deformation of stimuli and/or finger pads during the exploration may change the curvature distribution around participants' finger pads, as the surface is no longer a sphere. According to Hertz's contact theory [45], when exploring less curved surfaces (larger $R_{Stimulus}$ in equation 3), the deformation is larger (larger r in equation 3). This may explain the tendency for a lower accuracy.

The PSE indicates the curvature that participants subjectively feel equal to the corresponding reference curvature. To design accurate feedback with softness- and/or curvature-changing UIs, we should compensate for the difference between the real curvature and the curvature we expect participants will subjectively feel. For this reason, it is important to know whether systematic bias exists in any curvature and/or softness condition. Figure 8(a) shows the bias (i.e., the difference between PSE and the reference curvature) in each curvature and softness condition[5]. We can see that almost all error bars cross zero, except two in the flattest condition: For R_{ref}= 40 mm, the bias for the Shore 00-10 material is 3.23 mm (CI [1.60, 6.07]), and the bias of the rigid material is 1.59 mm (CI [0.46, 2.93]). This indicates that, in average, participants overestimated the curvature of rigid and softest stimuli in the flattest condition. I.e. participants felt that a rigid stimuli with an actual radius of 43.23 mm was a radius of 40 mm, and that participants felt that a Shore00-10 stimuli with an actual radius of 41.59 mm was a radius of 40 mm. This suggested that we should shift very soft (Shore 00-10) or rigid UIs' curvature to less curved when developing nearly flat UIs ($R \approx 40mm$).

In our experiment, the loss in accuracy occurred only in two extreme softness conditions (i.e., Shore 00-10 and rigid) when discriminating the lowest curvatures ($R \approx 40mm$). In addition, the participants in average overestimated the curvature under these conditions only. A larger $R_{Stimulus}$ can lead to larger deformation, and thus more bias. Furthermore, in the two extreme softness conditions, the large difference of softness between finger pads and stimulus lead to great deformation of either the stimuli (Shore 00-10 condition) or the finger pad (Rigid condition). This may explain the bias specific to these conditions. To better understand the overestimation of curvature for these conditions, future work can consider techniques for modeling the finger pad deformation when pressing on a rigid surface [38]. In addition, Figure 8 show a large variation among participants (blue dots). This may be explained by participant-dependent constants a and b in equation 2. Modeling techniques [38] may also help future understanding of the variation among participants.

6.4 Slower exploration and higher difficulty with softer material

There is no prior work on the exploration time of soft and curvy surfaces. We found that participants' exploration time in the softest condition was longer than the rigid condition for all curvatures (for the first and second stimulus, and their average). At the same time, the increase of the exploration time was slow when surfaces become softer. We can explain the slow increase in exploration time thanks to prior work. Neurophysiologists found that the SAI afferents play a major role in the cutaneous cues to encode the object shape (i.e., surface curvature in our experiment) [36, 46]. Prior work passively applied surfaces with different curvatures on participants' finger pads with controlled force and recorded the response of SAI afferents [36]. They found that the form of stimulus-response functions (i.e., the number of responses of SAI to different curvature of stimulus) measured over 1s were similar to the responses measured over 0.2s. This suggested our tactile mechanoreceptors are capable of rapidly encoding surface curvature information (within 0.2s). We hypothesize that the rapid shape-encoding capability of our mechanoreceptors might rapidly provide us with important cutaneous cues to estimate the curvature when our finger pads first touches a surface of any softness. On the contrary to passive perception [36], active curvature perception involved both cutaneous and kinesthetic cues [26]. We suppose the poorer kinesthetic cues with softer stimuli (i.e., the larger deformation of stimuli leads to less height change during exploration) may play a major role in the increase of the exploration time. The fact that mechanoreceptors rapidly provide cutaneous cues may explain the slow increase of exploration time.

These two types of cues involved in curvature perception may also explain why participants estimate the discrimination difficulty to be larger in softer conditions. Participants perceived both kinesthetic and cutaneous cues for curvature discrimination. Both are

[5]Figure 5 shows the distance between PSE and the reference curvature, i.e. the absolute value of the difference between PSE and the reference curvature. Figure 8 shows the difference, which can be either negative or positive.

affected by surface deformation and may hinder participants' discrimination. Future work can further study the impact of softness on participants' subjective difficulty to perceive curvature.

6.5 Different measures of softness

The softness of an object can express different physical quantity. First, the Young's modulus (E) of a material is the ratio between the pressure, i.e., the force per unit area (F/A) applied to the object and the strain, i.e., the relative deformation of the object ($\Delta l/l$): $E = \frac{F/A}{\Delta l/l}$ [21, 23]. The Young's modulus is a property of the material and is independent of the size and shape of the object.

Second, the stiffness (k) of an object is the ratio between the applied force and the deformation: $k = \frac{F}{\Delta l}$. The stiffness is a property of the object and depends on its shape and size. E.g., a silicone cylinder is half stiff as another silicone cylinder of the same material, if it has the same cross-sectional area but half the thickness [5].

Bergmann Tiest and Kappers compared these two measures of softness [5]: they demonstrate the major contribution of the Young's modulus (E) for softness discrimination (90% on average) and show the less important contribution of stiffness (k) (10% on average).

Both the Young's modulus and the stiffness can be measured through compression tests. Such tests control the force applied and measures the resulting displacement while the material is compressed. We conducted compression tests to measure the stiffness of our stimuli and the Young's modulus of our materials (Figure 9(a)). We used a SHIMADZU Autograph AGS-X Precision Universal Tester [76]. We followed the standard procedure with a loading speed of 0.2 mm/s [23]. Figure 9(a) presents the force-displacement curves that we measured with test specimens made of the same silicone as our soft stimuli. We used linear least-square regression to determine the slope of these curves (as in [5]). Although we computed the stiffness k as the slope –as in the definition– we notice that this is an approximation: Figure 9(a) shows that the stiffness of the Shore 00-10 test specimen is nonlinear, i.e., the slope is not constant during the whole test. However, the R^2 of the linear least-square regression is 0.86 for Shore 00-10, which is acceptable. The regression for all other curves have $R^2 \geq 0.96$. We found the stiffness of the stimuli to be $k_{00-10} = 1.54 Nmm^{-1}$, $k_{00-50} = 2.75 Nmm^{-1}$, and $k_{A-30} = 10.70 Nmm^{-1}$. We found the Young's modulus of each silicone to be $E_{00-10} = 0.088 MPa$, $E_{00-50} = 0.193 MPa$, and $E_{A-30} = 0.573 MPa$.

Third, the Shore hardness is another measure of the softness of a material, similar to the Young's modulus. Shore hardness can be easily measured with a durometer. Compared with a compression test machine, a durometer is portable, cheap and does not need expertise for its operation. A compression test (Figure 9(a)) compress the whole test specimen and measure the deflection of the whole specimen. In contrast, during a hardness test with a durometer, the surface of the indentor of a durometer, in contact with the test specimen, typically has a diameter ranging between 2.8 mm and 3.6 mm [6] [22]. The surface of the indentor of a durometer is smaller than the

[6] Different type of durometers have different dimension and form of indentor and used for measuring different scale of hardness. For example, a Shore 00 Durometer has a hemispherical indentor with a diameter of 2.38 mm and is typically used for testing extreme soft rubber, human and animal tissue, etc. A Shore A durometer has a truncated cone indentor with its top surface diameter of 0.79 mm and is typically used for testing harder rubber, leather, etc.

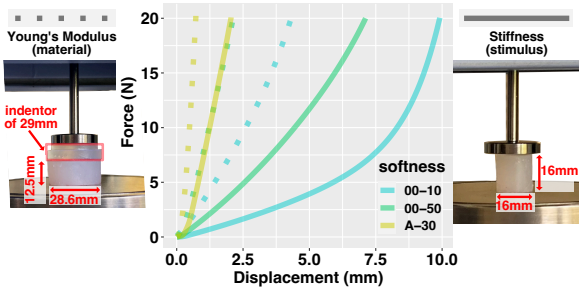

(a) Compression tests: Young's Modulus (dotted line, left) measured following the standard [23]. The indentor is 3D printed with rigid resin; The stiffness (solid line, right) measured with specimens with the same dimension as the stimuli used in our experiment.

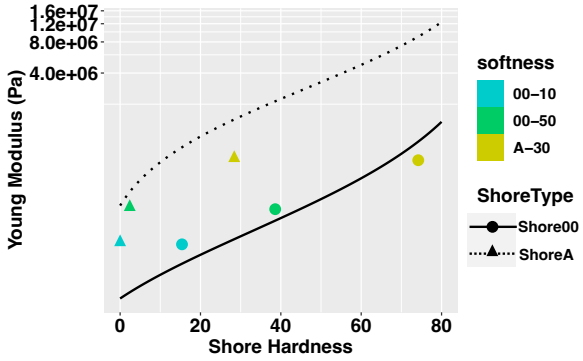

(b) Young's Modulus (predicted [57] and measured) vs. measured Shore 00 and Shore A hardness.

Figure 9: Measurements of the softness of our stimuli.

contact area between the participants' finger and the stimuli during our softness perception experiment. As opposed to the deflection of the whole specimen in a compression test (Figure 9(a)), the Shore hardness test measures the local deformation of the surface of the test specimen. There is no prior work studying participants' softness perception performance using Shore hardness as a measure of the softness of the stimuli. As a consequence, we do not know the respective contribution of the local deformation –Shore hardness– and the global deformation –Young's modulus– in users' softness perception. To help the design of soft UIs, designers can convert Young's modulus to Shore hardness and vice-versa [57]. The x axis of Figure 9(b) presents our measurements of the Shore hardness, with BAREISS HP Shore 00 and WALFRONT Shore-A durometers, following [23]. The y axis of Figure 9(b) presents the Young's modulus of the same object. The points in the graph show the Young's modulus we *measured* as in Figure 9(a). The lines in the graph show the Young's modulus we *predicted* using the existing conversion formula [57]. We found the Shore 00 hardness of each silicone to be $ShoreHardness00_{00-10} = 15$, $ShoreHardness00_{00-50} = 39$, and $ShoreHardness00_{A-30} = 74$. We found the ShoreA hardness of each silicone to be $ShoreHardnessA_{00-50} = 2$, and $ShoreHardnessA_{A-30} = 28$. The Shore 00-10 silicone is out range of a ShoreA durometer, which returns 0. Figure 9(b) shows that the Shore00 hardness highly

correlate with the measured Young's modulus (correlation coefficient $r \geq 0.98$). In contrast, the formulas [57] did not fit well our Shore00 (R^2=0.31). The low R^2 might come from the small sampling size, i.e., only three data points [7]. For the measurement of Shore A, we do not study the correlation coefficient (r) and R^2, as we had only two data points.

The non-linearity of stiffness during the compression (Figure 9(a)) impacts participants' perception of softness [67]. For this reason, we provide our whole force-displacement curve in addition to the three direct measurements of softness, i.e., Young's modulus, Stiffness, and Shore Hardness.

In our experiment, we chose the softness of our three soft stimuli based on the softness of the fingers pad, i.e., softer, as soft as, and harder than the index finger pad. We used the Shore hardness as a measure of softness, as it is convenient to measure on finger pads, contrary to other softness measurements. Meanwhile, there is no prior work on how the different measures of softness may impact our results. We provide different measures of softness, including Young's modulus, Stiffness, and Shore hardness (both Shore A and Shore 00) with force-displacement curves, which should help other designers to build their devices based on our results.

6.6 Linearity of curvature and softness

For each CURVATURE condition, the curvature of comparison stimuli was linearly distributed around the reference curvature, as explained in [30]. The curvature of our reference stimuli was not strictly linear: 100 m^{-1} for R_{ref}=10 mm, 50 m^{-1} for R_{ref}=20 mm and 25 m^{-1} for R_{ref}=40 mm. Figure 4(b) shows that the decrease of participants' curvature perception precision, i.e., the increase of JND, was exponential and non-linear. This suggests an exponential decrease of curvature perception precision when the stimuli become flatter, consistent with [37, 55, 70, 71]. Besides the three conditions of curvature we studied, i.e., R_{ref}=10 mm, 20mm, and 40 mm, Provancher et al. also studied the condition with R_{ref}=30 mm. We did not study the condition of R_{ref}=30 mm to reduce the total experiment time (around 4h). We found the exponent in the softness condition of the rigid stimuli was 1.45, which is similar to the exponent of 1.43 in [70, 71][7]. This suggested that we can use our power fitted curve (Figure 4(b)) to predict the JND in curvature condition not studied in our experiment despite the non-linearity of the distribution of the curvature of our stimuli, in particular with rigid stimuli whose curvature range is located between our studied values, i.e., R_{ref} from 10 mm to 40 mm.

In our three soft conditions, the JND also increased exponentially with respective exponent: 1.61 for Shore 00-10, 1.70 for Shore 00-50, and 1.76 for Shore A-30. This suggests a higher non-linear increase of JND with a softer surface: the softer the surface, the more the participants' curvature perception precision decrease as the surface becomes flat. The respective Young's modulus of the three soft stimuli were $E_{00-10} = 0.088$ MPa, $E_{00-50} = 0.193$ MPa, and $E_{A-30} = 0.573$ MPa, whose distribution is not linear. We noticed however that the exponents of the three JND curves (1.76 for Shore 00-10, 1.70 for Shore 00-50, 1.61 for Shore A-30) seem linearly distributed according to the three Young's modulus (R^2=0.92). However, further experiments are necessary to confirm this through the study of users' curvature perception with additional softness levels.

[7]The exponent is computed with the JND data provided in [70, 71].

7 GUIDELINES FOR SOFT CURVY DEVICES

This experiment provides quantitative data to design precise and accurate haptic feedback with soft curvy UIs. First, users can perceive with high precision and accuracy in the most curved condition ($R \approx 10$ mm) with any softness. Designers can use material of any softness to construct very curved UIs (radius ≈ 10 mm) for the most precise and accurate haptic feedback. In average, users can distinguish the surface curvature with a precision of 0.63 mm (CI=[0.53,0.78]) and an accuracy of 0.31 mm (CI=[0.26,0.38]). On the contrary, when UIs are less curved (radius ≥ 20 mm), designers should avoid using very soft material (softness < Shore 00-50) or dynamically stiffen the UI to reach a softness ≥ Shore 00-50. If the UI cannot change its softness, designers should provide a curvature change larger than the JND measured (Figure 4(b)) in corresponding softness and curvature condition, to ensure the curvature change is perceived. For example, a UI with a radius ≈ 20 mm should bend or flatten more than 2.72 mm if softer than Shore 00-50, and more than 2.00 mm if softer than Shore A-30.

Second, users can perceive the curvature of a very curved surface more accurately. The average accuracy of participants is 0.31 mm (CI=[0.26,0.38]) in R_{ref} = 10 mm; 0.90 mm (CI=[0.69,1.15]) in R_{ref} = 20 mm; 2.67 mm (CI=[2.13,3.49]) in R_{ref} = 40 mm. As a consequence, for better accuracy of curvature-based haptic feedback, designers should focus on the highest curvatures. At the same time, users can perceive the curvature of a surface with similar accuracy in all softnesses. This suggests that using stiff –or stiffening– material without changing the UI curvature will not improve users accuracy. When designing soft curvature-changing UIs, designers can fully focus on the interaction design and the application context, without worrying about the softness of a specific material: the softness will not have a significant impact on the output accuracy of the UI.

We observed a systematic curvature overestimation of 3.23 mm (CI=[1.60,6.07]) in the softest and flattest curvature. If designers cannot avoid these softness and curvature but still require accurate curvature feedback, they can offset by 3.23 mm the curvature of very soft and flat UIs (e.g., with a radius > 40 mm and softness ≈ Shore 00-10). Providing an even flatter surface (R=43.23 mm) will be perceived as a curvature of R= 40 mm.

Third, users need longer exploration time to perceive the curvature of softer surfaces. Users took in average 3.95s to explore a Shore 00-10 curvature vs. 3.39s to explore a rigid curvature. This suggests that stiffening the UIs [20] will enable more rapid feedback. If UIs cannot change their softness, the time between each refresh of UIs' curvature may need to be longer than the exploration time we measured. For instance, the curvature refresh rate of UIs softer than Shore 00-10 may need to be lower than 0.25 Hz, 0.27 Hz for UIs softer than Shore 00-50, and 0.28 Hz for UIs softer than Shore A-30 respectively. This is an opportunity for *slow* [39] ambiant on-body feedback supporting long-term interaction.

8 APPLICATIONS: BUILDING PRECISE AND ACCURATE INTERACTIVE DEVICES

Recent work explored interactive devices where the softness plays an important role [27]. We now show how our measurements of users' precision, accuracy and speed when perceiving the curvature of soft devices, inform the design of efficient haptic display through curvature and softness for such devices.

First, recent work presented technologies to vary participants' perception of softness of objects (e.g., Shore hardness of objects [84]). Recent work also proposed devices with different softness, e.g., different Shore hardness (e.g., [50]), different Young's modulus [67], or different stiffness [80]. We provide the measurements of the Young's modulus (Figures 9(a) and 9(b)), Shore hardness (Figure 9(b)), and stiffness (Figure 9(a)) used in our experiment, so that designers can directly apply our results when building their own soft devices. We summarize these finding in Table 1 to quickly enable precise and accurate curvature perception of future devices.

Second, we further distinguish three cases for the application of our results to current devices: (1) augmenting daily objects, building devices with (2) customized softness and shape, and (3) with changing softness and shape.

8.1 Augmented daily objects

Leveraging daily objects for interaction enable ubiquitous devices [29, 74]. VR systems can now scan users' surroundings to find daily objects with the most similar shape to the object manipulated in VR [41]. This reduces the visual-haptic mismatch, i.e., the mismatch between what users see in VR and what they touch and manipulate physically. Current technology (e.g., [3, 18]) also automatically measures the softness of objects. This can provide VR systems with softness information about surrounding daily objects. Our results help designers to fine-tune their algorithm to better choose soft objects in users' surroundings for haptic feedback in VR. For instance, when choosing a very soft and flat UIs (e.g., with R>40 mm and ~Shore 00-10), the algorithm can choose an even flatter surface (R=43.23 mm) to provide a curvature perception of R=40 mm.

In addition, prior work proposed a technique changing users' perceived softness of daily objects by controlling the expansion of the finger pad [84]. This device allows to change the perceived hardness ≥ Shore A-50 to ≈ Shore A-40. This range of softness is within the range of our experiment, i.e., between Shore A-30 and rigid. Their device leaves the center of the finger pad free, which allow users to directly perceive the curvature of the object. Our study informs future work with such devices by allowing the prediction of users' perception of the curvature of objects according to their perceived softness. For instance, when touching an object of curvature R=10mm with the device, designers can expect 0.53-0.58mm precision and 0.24-0.25mm accuracy in curvature perception.

8.2 Devices with custom softness and shape

3D printing eases the building of personal interactive devices [60] with complex geometric shape (e.g., [85]) and embedded interactive capabilities (e.g., [43]). 3D printing now also enables the customization of softness [50, 56, 58, 67, 85] to reach the desired haptic properties. Our results allow designers to predict users' accuracy and precision of curvature perception when manipulating 3D printed soft objects. For instance, OmniSoft [50] allows to build devices in the range of Shore A-02 to Shore A-30 –a range included in our experiment. Our results now extend Omnisoft with information about users perception of the object's local curvature depending on its local softness.

Our results can also be readily used together with a new model that converts a softness, e.g., a Young's modulus, into an infill geometry ensuring the same perceived softness [67]. Using our measurements of the Young's modulus (Table 1) as an input to the model, our results now extend this prior work with the corresponding users' precision and accuracy in perception of the object's local curvature depending on its local softness.

8.3 Devices with changing softness and shape

Prior work enabled devices capable of changing their softness, e.g., through jamming [20, 80]. Adding a jamming layer on top of an existing shape-changing device such as LayerPump [28], dynamically changeable buttons [32, 40], the inflatable hemispherical display [83], PneUI [97], AirPinch [33], MultiJam [96], Pneumatic Auxetics [16], StringTouch [73], or PneuSeries [8], allows building devices providing haptic feedback through both softness and shape. The jamming layer can follow the shape of the shape-changing device, thanks to its malleability prior to jamming [80, 97]. By controlling the vacuum level in the jamming layer [20, 80], a device can change its softness: the higher the vacuum level, the stiffer the jamming layer.

Our results can be used to refine the design of such devices. We illustrate this on the example of a device that changes its curvature and softness through pneumatic actuation and a jamming layer [80]. Figure 10 shows two sets of force-displacement curves: one (in gray) that we reproduce from [80], and the other (in color) that we measured as in [80] with our specimen made of silicone of different softness. To measure the force-displacement, we used the same indentor as in [80], i.e., a printed rigid sphere with a diameter of 9.5 mm (Figure 10, right). We can see in Figure 10 that the force-displacement measurements of the jamming layer at the 15 inHg level of vacuum overlaps with our Shore A-30 specimen measurements. In addition, the 0 inHg level of vacuum partially overlaps with Shore 00-10 specimen measurements when the displacement of the indentor is < 5 mm. We can also see that the measurements of our Shore 00-50 lie between the jamming layer at 0 and 1 inHg. This suggests that a jamming layer with a vacuum level between 0 and 1 inHg might produce force-displacement measurements that overlap or partially overlaps with the measurements of our Shore 00-50. Based on Figure 10, we can now predict the precision and accuracy in curvature perception of such a device changing its curvature and softness. For instance, a curved UI with a jamming layer like [80] at 15 inHg of vacuum should provide users with similar curvature perception precision and accuracy as our stimuli in Shore A-30 condition (Table 1). When the vacuum level is at 1 inHg, the UI should provide better curvature perception precision than our Shore 00-50 stimuli, in particular when the UI surface is very flat (e.g., with a radius > 40 mm). When the vacuum level is at 0 inHg, the UI should provide similar curvature perception precision and accuracy as our Shore 00-10 stimuli, if users' fingers do not press too deep into the UI (e.g., ≤ 5 mm).

Table 1: Correspondence table for designers of novel soft and curvy devices.

SOFTNESS					CURVATURE (radius in mm)	PRECISION (mm)	ACCURACY (mm)	TIME (s)
Shore hardness		Stiffness (N.mm-1)	Young's modulus (MPa)	Jamming vacuum (inHg) [80]				
00-10	N.A.	1.54	0.088	0	10	0.75	0.41	3.46
					20	2.63	1.13	4.04
					40	8.61	3.46	4.37
00-50	A-02	2.75	0.193		10	0.68	0.34	3.43
					20	2.72	1.03	3.79
					40	7.14	3.01	3.80
00-74	A-30	10.70	0.573	15	10	0.53	0.24	3.20
					20	2.03	0.58	3.65
					40	4.98	2.24	3.68
Rigid					10	0.58	0.25	3.21
					20	1.97	0.83	3.54
					40	4.31	1.95	3.98

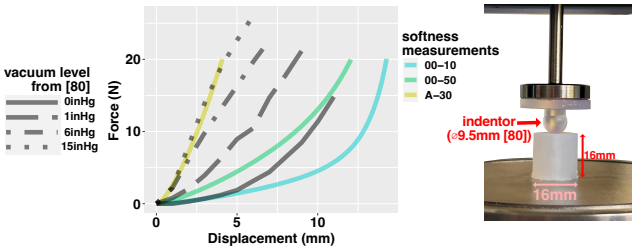

Figure 10: (Left) Force displacement curves resulting from (right) compression tests with a 3D printed spherical indentor as in [80]. Colored lines show our results on a specimen with the same dimensions as the stimuli used in our experiment. Gray lines show prior results [80] from compression test on a jamming layer. The level of vacuum are expressed in inches of mercury (inHg). The larger the value, the higher the vacuum and the stiffer the UI.

9 CONCLUSION AND FUTURE WORK

This paper presents an experiment determining the accuracy (point of subjective equality), the precision (just noticeable difference) and the exploration time when perceiving curvature across four levels of softness of a UI. Results show (1) similar accuracy and precision when discriminating very curved surfaces in all softness conditions, (2) decreasing precision with softer curved surfaces when discriminating less curved surfaces, and (3) decreasing exploration speed with softer surfaces in all curvature levels. Our results show the potential of using soft materials to build curvature-changing UIs for precise and accurate feedback. We provide guidelines for the design of soft curvature-changing UIs in a large range of curvatures and a large range of softnesses. The HCI community can readily build on top of this work to design soft curvature-changing UIs.

Our work can be extended by studying the possible combined impact of air pressure inside inflatable soft UIs and the softness of their materials. Another exciting avenue for future work is the study of concave surfaces, although convex surfaces are currently more common (e.g., PneUI [97] and Pneumatibles [32]). Future work should also study the impact of shape on softness perception, the absolute estimation of the curvature (magnitude estimation), and the perception of continuous change in curvature, e.g., when users keep their finger on top of the UI and experience a transition between two curvatures. Another important lead for future work is the study of user experience with soft curvature feedback in ecological settings.

ACKNOWLEDGMENTS

We would like to thank Benoit Roman, Pierre Sailler, Maud Marchal, François Bérard, Anne Roudaut, Thomas Pietzrak, Alexis Sanson and FabMSTIC. This work was supported by CNRS (80 Prime MeMorI) and the French National Research Agency (ANR-21-CE33-0018).

REFERENCES

[1] Jason Alexander, Anne Roudaut, Jürgen Steimle, Kasper Hornbæk, Miguel Bruns Alonso, Sean Follmer, and Timothy Merritt. 2018. *Grand Challenges in Shape-Changing Interface Research.* Association for Computing Machinery, New York, NY, USA, 1–14. https://doi.org/10.1145/3173574.3173873

[2] American Psychological Association et al. 2019. *Publication Manual of the American Psychological Association, (2020).* American Psychological Association, Washington, D.C., United States.

[3] Fariborz Baghaei Naeini, Aamna M. AlAli, Raghad Al-Husari, Amin Rigi, Mohammad K. Al-Sharman, Dimitrios Makris, and Yahya Zweiri. 2020. A Novel Dynamic-Vision-Based Approach for Tactile Sensing Applications. *IEEE Transactions on Instrumentation and Measurement* 69, 5 (2020), 1881–1893. https://doi.org/10.1109/TIM.2019.2919354

[4] Jose Barreiros, Houston Claure, Bryan Peele, Omer Shapira, Josef Spjut, David Luebke, Malte Jung, and Robert Shepherd. 2019. Fluidic Elastomer Actuators for Haptic Interactions in Virtual Reality. *IEEE Robotics and Automation Letters* 4, 2 (2019), 277–284. https://doi.org/10.1109/LRA.2018.2888628

[5] Wouter M. Bergmann Tiest and Astrid M. L. Kappers. 2009. Cues for Haptic Perception of Compliance. *IEEE Transactions on Haptics* 2, 4 (2009), 189–199. https://doi.org/10.1109/TOH.2009.16

[6] A. Bicchi, E.P. Scilingo, and D. De Rossi. 2000. Haptic discrimination of softness in teleoperation: the role of the contact area spread rate. *IEEE Transactions on Robotics and Automation* 16, 5 (2000), 496–504. https://doi.org/10.1109/70.880800

[7] Mohamad Adam Bujang, Nadiah Sa'at, Tg Mohd Ikhwan Tg Abu Bakar, et al. 2017. Determination of minimum sample size requirement for multiple linear regression and analysis of covariance based on experimental and non-experimental studies.

Epidemiology, Biostatistics, and Public Health 14, 3 (2017), 9 pages. https://doi.org/10.2427/12117

[8] Yu-Wen Chen, Wei-Ju Lin, Yi Chen, and Lung-Pan Cheng. 2021. PneuSeries: 3D Shape Forming with Modularized Serial-Connected Inflatables. In *The 34th Annual ACM Symposium on User Interface Software and Technology* (Virtual Event, USA) *(UIST '21)*. Association for Computing Machinery, New York, NY, USA, 431–440. https://doi.org/10.1145/3472749.3474760

[9] G. Cini, A. Frisoli, S. Marcheschi, F. Salsedo, and M. Bergamasco. 2005. A novel fingertip haptic device for display of local contact geometry. In *First Joint Eurohaptics Conference and Symposium on Haptic Interfaces for Virtual Environment and Teleoperator Systems. World Haptics Conference.* Institute of Electrical and Electronics Engineers, Pisa, Italy, 602–605. https://doi.org/10.1109/WHC.2005.16

[10] Kerstyn Comley and Norman A. Fleck. 2010. A micromechanical model for the Young's modulus of adipose tissue. *International Journal of Solids and Structures* 47, 21 (2010), 2982–2990. https://doi.org/10.1016/j.ijsolstr.2010.07.001

[11] Melia Condon, Ingvars Birznieks, Kathryn Hudson, David K. Chelvanayagam, David Mahns, Håkan Olausson, and Vaughan G. Macefield. 2014. Differential sensitivity to surface compliance by tactile afferents in the human finger pad. *Journal of Neurophysiology* 111, 6 (2014), 1308–1317. https://doi.org/10.1152/jn.00589.2013 arXiv:https://doi.org/10.1152/jn.00589.2013 PMID: 24371291.

[12] Kiran Dandekar, Balasundar I. Raju, and Mandayam A. Srinivasan. 2003. 3-D Finite-Element Models of Human and Monkey Fingertips to Investigate the Mechanics of Tactile Sense . *Journal of Biomechanical Engineering* 125, 5 (10 2003), 682–691. https://doi.org/10.1115/1.1613673 arXiv:https://asmedigitalcollection.asme.org/biomechanical/article-pdf/125/5/682/5767639/682_1.pdf

[13] Kurtis Danyluk, Bernhard Jenny, and Wesley Willett. 2019. Look-From Camera Control for 3D Terrain Maps. In *Proceedings of the 2019 CHI Conference on Human Factors in Computing Systems* (Glasgow, Scotland Uk) *(CHI '19)*. Association for Computing Machinery, New York, NY, USA, 1–12. https://doi.org/10.1145/3290605.3300594

[14] Ruta Desai, Fraser Anderson, Justin Matejka, Stelian Coros, James McCann, George Fitzmaurice, and Tovi Grossman. 2019. Geppetto: Enabling Semantic Design of Expressive Robot Behaviors. In *Proceedings of the 2019 CHI Conference on Human Factors in Computing Systems* (Glasgow, Scotland Uk) *(CHI '19)*. Association for Computing Machinery, New York, NY, USA, 1–14. https://doi.org/10.1145/3290605.3300599

[15] Pierre Dragicevic. 2016. Fair statistical communication in HCI. In *Modern statistical methods for HCI*. Springer, Berlin, Germany, 291–330. https://doi.org/10.1007/978-3-319-26633-6_13

[16] Soya Eguchi, Claire Okabe, Mai Ohira, and Hiroya Tanaka. 2022. Pneumatic Auxetics: Inverse Design and 3D Printing of Auxetic Pattern for Pneumatic Morphing. In *Extended Abstracts of the 2022 CHI Conference on Human Factors in Computing Systems* (New Orleans, LA, USA) *(CHI EA '22)*. Association for Computing Machinery, New York, NY, USA, Article 435, 7 pages. https://doi.org/10.1145/3491101.3519801

[17] Andrew Engel. 2017. *Validation and Modeling of a Subject-Driven Device for In Vivo Finger Indentation Using a Finger Mimic.* Ph.D. Dissertation. University of Cincinnati. https://etd.ohiolink.edu/apexprod/rws_etd/send_file/send?accession=ucin1491557931643749&disposition=inline

[18] Zackory Erickson, Eliot Xing, Bharat Srirangam, Sonia Chernova, and Charles C. Kemp. 2020. Multimodal Material Classification for Robots using Spectroscopy and High Resolution Texture Imaging. In *2020 IEEE/RSJ International Conference on Intelligent Robots and Systems (IROS)*. Institute of Electrical and Electronics Engineers, Las Vegas, NV, USA, 10452–10459. https://doi.org/10.1109/IROS45743.2020.9341165

[19] Vincent Falanga and Brian Bucalo. 1993. Use of a durometer to assess skin hardness. *Journal of the American Academy of Dermatology* 29, 1 (1993), 47–51. https://doi.org/10.1016/0190-9622(93)70150-R

[20] Sean Follmer, Daniel Leithinger, Alex Olwal, Nadia Cheng, and Hiroshi Ishii. 2012. Jamming User Interfaces: Programmable Particle Stiffness and Sensing for Malleable and Shape-Changing Devices. In *Proceedings of the 25th Annual ACM Symposium on User Interface Software and Technology* (Cambridge, Massachusetts, USA) *(UIST '12)*. Association for Computing Machinery, New York, NY, USA, 519–528. https://doi.org/10.1145/2380116.2380181

[21] American Society for Testing and Materials. 2010. Standard Test Method for Young's Modulus, Tangent Modulus, and Chord Modulus. In *ASTM Volume 03.01: Metals – Mechanical Testing; Elevated And Low-temperature Tests; Metallography*. ASTM West Conshohocken, American Society for Testing and Materials, West Conshohocken, Pennsylvania, United States, 7. https://doi.org/10.1520/E0111-04R10

[22] American Society for Testing and Materials. 2015. ASTM D2240-15 standard test method for rubber property: durometer hardness. In *ASTM Volume 09.01: Rubber, Natural And Synthetic — General Test Methods; Carbon Black*. ASTM West Conshohocken, American Society for Testing and Materials, West Conshohocken, Pennsylvania, United States, 13. https://doi.org/10.1520/D2240-15

[23] American Society for Testing and Materials. 2018. Standard Test Methods for Rubber Properties in Compression. In *ASTM Volume 09.01: Rubber, Natural And Synthetic — General Test Methods; Carbon Black*. ASTM West Conshohocken, American Society for Testing and Materials, West Conshohocken, Pennsylvania, United States, 4. https://doi.org/10.1520/D0575-91R18

[24] Gabriele Frediani and Federico Carpi. 2020. Tactile display of softness on fingertip. *Scientific reports* 10, 1 (2020), 1–10. https://doi.org/10.1038/s41598-020-77591-0

[25] Robert M Friedman, Kim D Hester, Barry G Green, and Robert H LaMotte. 2008. Magnitude estimation of softness. *Experimental brain research* 191, 2 (2008), 133–142. https://doi.org/10.1007/s00221-008-1507-5

[26] A. Frisoli, M. Solazzi, F. Salsedo, and M. Bergamasco. 2008. A Fingertip Haptic Display for Improving Curvature Discrimination. *Presence: Teleoperators and Virtual Environments* 17, 6 (12 2008), 550–561. https://doi.org/10.1162/pres.17.6.550 arXiv:https://direct.mit.edu/pvar/article-pdf/17/6/550/1624873/pres.17.6.550.pdf

[27] Bruno Fruchard, Paul Strohmeier, Roland Bennewitz, and Jürgen Steimle. 2021. Squish This: Force Input on Soft Surfacesfor Visual Targeting Tasks. In *Proceedings of the 2021 CHI Conference on Human Factors in Computing Systems* (Yokohama, Japan) *(CHI '21)*. Association for Computing Machinery, New York, NY, USA, Article 219, 9 pages. https://doi.org/10.1145/3411764.3445623

[28] Juri Fujii, Satoshi Nakamaru, and Yasuaki Kakehi. 2021. LayerPump: Rapid Prototyping of Functional 3D Objects with Built-in Electrohydrodynamics Pumps Based on Layered Plates. In *Proceedings of the Fifteenth International Conference on Tangible, Embedded, and Embodied Interaction* (Salzburg, Austria) *(TEI '21)*. Association for Computing Machinery, New York, NY, USA, Article 48, 7 pages. https://doi.org/10.1145/3430524.3442453

[29] Kaori Fujinami. 2009. Implicit Interaction with Daily Objects: Applications and Issues. In *Proceedings of the 3rd International Universal Communication Symposium* (Tokyo, Japan) *(IUCS '09)*. Association for Computing Machinery, New York, NY, USA, 163–168. https://doi.org/10.1145/1667780.1667813

[30] George A Gescheider. 2016. *Psychophysics: the fundamentals* (third ed.). Routledge, Milton Park, Abingdon-on-Thames, Oxfordshire, England, UK. 46–54,183–186 pages. https://www.routledge.com/Psychophysics-The-Fundamentals/Gescheider/p/book/9781138984158

[31] James J Gibson. 1962. Observations on active touch. *Psychological review* 69, 6 (1962), 477.

[32] Kristian Gohlke, Eva Hornecker, and Wolfgang Sattler. 2016. Pneumatibles: Exploring Soft Robotic Actuators for the Design of User Interfaces with Pneumotactile Feedback. In *Proceedings of the TEI '16: Tenth International Conference on Tangible, Embedded, and Embodied Interaction* (Eindhoven, Netherlands) *(TEI '16)*. Association for Computing Machinery, New York, NY, USA, 308–315. https://doi.org/10.1145/2839462.2839489

[33] Kristian Gohlke, Wolfgang Sattler, and Eva Hornecker. 2022. AirPinch – An Inflatable Touch Fader with Pneumatic Tactile Feedback. In *Sixteenth International Conference on Tangible, Embedded, and Embodied Interaction* (Daejeon, Republic of Korea) *(TEI '22)*. Association for Computing Machinery, New York, NY, USA, Article 64, 6 pages. https://doi.org/10.1145/3490149.3505568

[34] AW Goodwin, KT John, and AH Marceglia. 1991. Tactile discrimination of curvature by humans using only cutaneous information from the fingerpads. *Experimental brain research* 86, 3 (1991), 663–672. https://doi.org/10.1007/BF00230540

[35] AW Goodwin and HE Wheat. 1992. Human tactile discrimination of curvature when contact area with the skin remains constant. *Experimental brain research* 88, 2 (1992), 447–450. https://doi.org/10.1007/BF02259120

[36] A. W. Goodwin, V. G. Macefield, and J. W. Bisley. 1997. Encoding of Object Curvature by Tactile Afferents From Human Fingers. *Journal of Neurophysiology* 78, 6 (1997), 2881–2888. https://doi.org/10.1152/jn.1997.78.6.2881 arXiv:https://doi.org/10.1152/jn.1997.78.6.2881 PMID: 9405508.

[37] Ian E Gordon and Victoria Morison. 1982. The haptic perception of curvature. *Perception & psychophysics* 31, 5 (1982), 446–450. https://doi.org/10.3758/BF03204854

[38] David Gueorguiev, Dimitrios Tzionas, Claudio Pacchierotti, Michael J. Black, and Katherine J. Kuchenbecker. 2018. Statistical Modelling of Fingertip Deformations and Contact Forces during Tactile Interaction. Extended abstract presented at the Hand, Brain and Technology conference (HBT).

[39] Lars Hallnäs and Johan Redström. 2001. Slow Technology – Designing for Reflection. *Personal Ubiquitous Comput.* 5, 3 (jan 2001), 201–212. https://doi.org/10.1007/PL00000019

[40] Chris Harrison and Scott E. Hudson. 2009. *Providing Dynamically Changeable Physical Buttons on a Visual Display.* Association for Computing Machinery, New York, NY, USA, 299–308. https://doi.org/10.1145/1518701.1518749

[41] Anuruddha Hettiarachchi and Daniel Wigdor. 2016. Annexing Reality: Enabling Opportunistic Use of Everyday Objects as Tangible Proxies in Augmented Reality. In *Proceedings of the 2016 CHI Conference on Human Factors in Computing Systems* (San Jose, California, USA) *(CHI '16)*. Association for Computing Machinery, New York, NY, USA, 1957–1967. https://doi.org/10.1145/2858036.2858134

[42] Seiji Inaba, Shigeru Fujino, and Kenji Morinaga. 1999. Young's Modulus and Compositional Parameters of Oxide Glasses. *Journal of the American Ceramic Society* 82, 12 (1999), 3501–3507. https://doi.org/10.1111/j.1151-2916.1999.tb02272.x arXiv:https://ceramics.onlinelibrary.wiley.com/doi/pdf/10.1111/j.1151-2916.1999.tb02272.x

[43] Yoshio Ishiguro and Ivan Poupyrev. 2014. 3D Printed Interactive Speakers. In *Proceedings of the SIGCHI Conference on Human Factors in Computing Systems*

(Toronto, Ontario, Canada) *(CHI '14)*. Association for Computing Machinery, New York, NY, USA, 1733–1742. https://doi.org/10.1145/2556288.2557046

[44] Yvonne Jansen, Jonas Schjerlund, and Kasper Hornbæk. 2019. Effects of Locomotion and Visual Overview on Spatial Memory When Interacting with Wall Displays. In *Proceedings of the 2019 CHI Conference on Human Factors in Computing Systems* (Glasgow, Scotland Uk) *(CHI '19)*. Association for Computing Machinery, New York, NY, USA, 1–12. https://doi.org/10.1145/3290605.3300521

[45] K. L. Johnson. 1985. *Normal contact of elastic solids – Hertz theory.* Cambridge University Press, Cambridge, United Kingdom, 84–106. https://doi.org/10.1017/CBO9781139171731.005

[46] Kenneth O Johnson. 2001. The roles and functions of cutaneous mechanoreceptors. *Current Opinion in Neurobiology* 11, 4 (2001), 455–461. https://doi.org/10.1016/S0959-4388(00)00234-8

[47] Kenichi Kanatani and Prasanna Rangarajan. 2011. Hyper least squares fitting of circles and ellipses. *Computational Statistics & Data Analysis* 55, 6 (2011), 2197–2208. https://doi.org/10.1016/j.csda.2010.12.012

[48] Elio Keddisseh, Marcos Serrano, and Emmanuel Dubois. 2021. KeyTch: Combining the Keyboard with a Touchscreen for Rapid Command Selection on Toolbars. In *Proceedings of the 2021 CHI Conference on Human Factors in Computing Systems* (Yokohama, Japan) *(CHI '21)*. Association for Computing Machinery, New York, NY, USA, Article 191, 13 pages. https://doi.org/10.1145/3411764.3445288

[49] Hyunyoung Kim, Celine Coutrix, and Anne Roudaut. 2018. *Morphees+: Studying Everyday Reconfigurable Objects for the Design and Taxonomy of Reconfigurable UIs.* Association for Computing Machinery, New York, NY, USA, 1–14. https://doi.org/10.1145/3173574.3174193

[50] Jeeeun Kim, Qingnan Zhou, Amanda Ghassaei, and Xiang 'Anthony' Chen. 2021. OmniSoft: A Design Tool for Soft Objects by Example. In *Proceedings of the Fifteenth International Conference on Tangible, Embedded, and Embodied Interaction* (Salzburg, Austria) *(TEI '21)*. Association for Computing Machinery, New York, NY, USA, Article 15, 13 pages. https://doi.org/10.1145/3430524.3440634

[51] Umut Koçak, Karljohan Palmerius, Camilla Forsell, Anders Ynnerman, and Matthew Cooper. 2011. Analysis of the JND of Stiffness in Three Modes of Comparison. In *Proceedings of Haptic and Audio Interaction Design - 6th International Workshop, HAID 2011, Kusatsu, Japan, August 25-26*, Vol. 6851. Springer, Berlin, Germany, 22–31. https://doi.org/10.1007/978-3-642-22950-3_3

[52] Pin-Sung Ku, Kunpeng Huang, and Cindy Hsin-Liu Kao. 2022. Patch-O: Deformable Woven Patches for On-Body Actuation. In *Proceedings of the 2022 CHI Conference on Human Factors in Computing Systems* (New Orleans, LA, USA) *(CHI '22)*. Association for Computing Machinery, New York, NY, USA, Article 615, 12 pages. https://doi.org/10.1145/3491102.3517633

[53] Caitlin Kuhlman, Diana Doherty, Malika Nurbekova, Goutham Deva, Zarni Phyo, Paul-Henry Schoenhagen, MaryAnn VanValkenburg, Elke Rundensteiner, and Lane Harrison. 2019. Evaluating Preference Collection Methods for Interactive Ranking Analytics. In *Proceedings of the 2019 CHI Conference on Human Factors in Computing Systems* (Glasgow, Scotland Uk) *(CHI '19)*. Association for Computing Machinery, New York, NY, USA, 1–11. https://doi.org/10.1145/3290605.3300742

[54] Susan J Lederman and Roberta L Klatzky. 2009. Haptic perception: A tutorial. *Attention, Perception, & Psychophysics* 71, 7 (2009), 1439–1459. https://doi.org/10.3758/APP.71.7.1439

[55] Stefan Louw, Astrid ML Kappers, and Jan J Koenderink. 2000. Haptic detection thresholds of Gaussian profiles over the whole range of spatial scales. *Experimental brain research* 132, 3 (2000), 369–374. https://doi.org/10.1007/s002210000350

[56] Jonàs Martínez, Jérémie Dumas, and Sylvain Lefebvre. 2016. Procedural Voronoi Foams for Additive Manufacturing. *ACM Trans. Graph.* 35, 4, Article 44 (jul 2016), 12 pages. https://doi.org/10.1145/2897824.2925922

[57] A. W. Mix and A. J. Giacomin. 2011. Dimensionless Durometry. *Polymer-Plastics Technology and Engineering* 50, 3 (2011), 288–296. https://doi.org/10.1080/03602559.2010.531867 arXiv:https://doi.org/10.1080/03602559.2010.531867

[58] Motoki Miyoshi, Parinya Punpongsanon, Daisuke Iwai, and Kosuke Sato. 2021. SoftPrint: Investigating Haptic Softness Perception of 3D Printed Soft Object in FDM 3D Printers. In *NIP & Digital Fabrication Conference*. Society for Imaging Science and Technology, Society for Imaging Science and Technology, Springfield, Virginia, 78–85. https://doi.org/10.2352/J.ImagingSci.Technol.2021.65.4.040406

[59] Alessandro Moscatelli, Maura Mezzetti, and Francesco Lacquaniti. 2012. Modeling psychophysical data at the population-level: The generalized linear mixed model. *Journal of Vision* 12, 11 (10 2012), 26–26. https://doi.org/10.1167/12.11.26 arXiv:https://arvojournals.org/arvo/content_public/journal/jov/933489/i1534-7362-12-11-26.pdf

[60] Stefanie Mueller. 2017. 3D Printing for Human-Computer Interaction. *Interactions* 24, 5 (aug 2017), 76–79. https://doi.org/10.1145/3125399

[61] Thomas Muender, Anke Verena Reinschluessel, Daniela Salzmann, Thomas Lück, Andrea Schenk, Dirk Weyhe, Tanja Döring, and Rainer Malaka. 2022. Evaluating Soft Organ-Shaped Tangibles for Medical Virtual Reality. In *Extended Abstracts of the 2022 CHI Conference on Human Factors in Computing Systems* (New Orleans, LA, USA) *(CHI EA '22)*. Association for Computing Machinery, New York, NY, USA, Article 237, 8 pages. https://doi.org/10.1145/3491101.3519715

[62] Pranathi Mylavarapu, Adil Yalcin, Xan Gregg, and Niklas Elmqvist. 2019. Ranked-List Visualization: A Graphical Perception Study. In *Proceedings of the 2019 CHI Conference on Human Factors in Computing Systems* (Glasgow, Scotland Uk) *(CHI '19)*. Association for Computing Machinery, New York, NY, USA, 1–12. https://doi.org/10.1145/3290605.3300422

[63] Ryosuke Nakayama, Ryo Suzuki, Satoshi Nakamaru, Ryuma Niiyama, Yoshihiro Kawahara, and Yasuaki Kakehi. 2019. MorphIO: Entirely Soft Sensing and Actuation Modules for Programming Shape Changes through Tangible Interaction. In *Proceedings of the 2019 on Designing Interactive Systems Conference* (San Diego, CA, USA) *(DIS '19)*. Association for Computing Machinery, New York, NY, USA, 975–986. https://doi.org/10.1145/3322276.3322337

[64] C Oprişan, V Cârlescu, A Barnea, Gh Prisacaru, D N Olaru, and Gh Plesu. 2016. Experimental determination of the Young's modulus for the fingers with application in prehension systems for small cylindrical objects. *IOP Conference Series: Materials Science and Engineering* 147 (aug 2016), 012058. https://doi.org/10.1088/1757-899x/147/1/012058

[65] Mariola Pawlaczyk, Monika Lelonkiewicz, and Michał Wieczorowski. 2013. Review papersAge-dependent biomechanical properties of the skin. *Advances in Dermatology and Allergology/Postępy Dermatologii i Alergologii* 30, 5 (2013), 302–306. https://doi.org/10.5114/pdia.2013.38359

[66] V.C. Pinto, Tiago Ramos, Sofia Alves, J. Xavier, Paulo Tavares, P.M.G.P. Moreira, and Rui Miranda Guedes. 2015. Comparative Failure Analysis of PLA, PLA/GNP and PLA/CNT-COOH Biodegradable Nanocomposites thin Films. *Procedia Engineering* 114 (2015), 635–642. https://doi.org/10.1016/j.proeng.2015.08.004 ICSI 2015 The 1st International Conference on Structural Integrity Funchal, Madeira, Portugal 1st to 4th September, 2015.

[67] Michal Piovarči, David I. W. Levin, Jason Rebello, Desai Chen, Roman Ďurikovič, Hanspeter Pfister, Wojciech Matusik, and Piotr Didyk. 2016. An Interaction-Aware, Perceptual Model for Non-Linear Elastic Objects. *ACM Trans. Graph.* 35, 4, Article 55 (jul 2016), 13 pages. https://doi.org/10.1145/2897824.2925885

[68] Sylvia C Pont, Astrid ML Kappers, and Jan J Koenderink. 1997. Haptic curvature discrimination at several regions of the hand. *Perception & Psychophysics* 59, 8 (1997), 1225–1240. https://doi.org/10.3758/BF03214210

[69] Sylvia C Pont, Astrid ML Kappers, and Jan J Koenderink. 1999. Similar mechanisms underlie curvature comparison by static and dynamic touch. *Perception & Psychophysics* 61, 5 (1999), 874–894. https://doi.org/10.3758/BF03206903

[70] William Ronald Provancher. 2003. *On tactile sensing and display.* Stanford University, Stanford, California,USA. http://www-cdr.stanford.edu/DML/publications/provancher_thesis.pdf

[71] William R. Provancher, Katherine J. Kuchenbecker, Günter Niemeyer, and Mark R. Cutkosky. 2005. Perception of Curvature and Object Motion via Contact Location Feedback. In *Robotics Research. The Eleventh International Symposium*, Paolo Dario and Raja Chatila (Eds.). Springer Berlin Heidelberg, Berlin, Heidelberg, 456–465. https://doi.org/10.1007/11008941_49

[72] Isabel P. S. Qamar, Rainer Groh, David Holman, and Anne Roudaut. 2018. *HCI Meets Material Science: A Literature Review of Morphing Materials for the Design of Shape-Changing Interfaces.* Association for Computing Machinery, New York, NY, USA, 1–23. https://doi.org/10.1145/3173574.3173948

[73] Beat Rossmy, Sonja Rümelin, and Alexander Wiethoff. 2021. StringTouch - From String Instruments towards New Interface Morphologies. In *Proceedings of the Fifteenth International Conference on Tangible, Embedded, and Embodied Interaction* (Salzburg, Austria) *(TEI '21)*. Association for Computing Machinery, New York, NY, USA, Article 9, 10 pages. https://doi.org/10.1145/3430524.3440628

[74] Munehiko Sato, Ivan Poupyrev, and Chris Harrison. 2012. Touché: Enhancing Touch Interaction on Humans, Screens, Liquids, and Everyday Objects. In *Proceedings of the SIGCHI Conference on Human Factors in Computing Systems* (Austin, Texas, USA) *(CHI '12)*. Association for Computing Machinery, New York, NY, USA, 483–492. https://doi.org/10.1145/2207676.2207743

[75] Enzo Pasquale Scilingo, Matteo Bianchi, Giorgio Grioli, and Antonio Bicchi. 2010. Rendering Softness: Integration of Kinesthetic and Cutaneous Information in a Haptic Device. *IEEE Transactions on Haptics* 3, 2 (2010), 109–118. https://doi.org/10.1109/TOH.2010.2

[76] SHIMADZU. 2022. SHIMADZU Autograph AGS-X Precision Universal Tester. https://www.shimadzu.eu/ags-x-series-0 (last retrieved February 3, 2023).

[77] Gurpreet Singh and Arnab Chanda. 2021. Mechanical properties of whole-body soft human tissues: a review. *Biomedical Materials* 16, 6 (oct 2021), 062004. https://doi.org/10.1088/1748-605x/ac2b7a

[78] M. A. Srinivasan and R. H. LaMotte. 1995. Tactual discrimination of softness. *Journal of Neurophysiology* 73, 1 (1995), 88–101. https://doi.org/10.1152/jn.1995.73.1.88 arXiv:https://doi.org/10.1152/jn.1995.73.1.88 PMID: 7714593.

[79] Andrew A. Stanley, James C. Gwilliam, and Allison M. Okamura. 2013. Haptic jamming: A deformable geometry, variable stiffness tactile display using pneumatics and particle jamming. In *2013 World Haptics Conference (WHC)*. Institute of Electrical and Electronics Engineers, Daejeon, Korea (South), 25–30. https://doi.org/10.1109/WHC.2013.6548379

[80] Andrew A. Stanley and Allison M. Okamura. 2015. Controllable Surface Haptics via Particle Jamming and Pneumatics. *IEEE Transactions on Haptics* 8, 1 (2015), 20–30. https://doi.org/10.1109/TOH.2015.2391093

[81] Andrew A. Stanley and Allison M. Okamura. 2017. Deformable Model-Based Methods for Shape Control of a Haptic Jamming Surface. *IEEE Transactions on Visualization and Computer Graphics* 23, 2 (2017), 1029–1041. https://doi.org/10.1109/TVCG.2016.2525788

[82] Stanley Smith Stevens. 1966. Matching functions between loudness and ten other continua1. *Perception & Psychophysics* 1, 1 (1966), 5–8. https://doi.org/10.3758/BF03207813

[83] Andrew Stevenson, Christopher Perez, and Roel Vertegaal. 2010. An Inflatable Hemispherical Multi-Touch Display. In *Proceedings of the Fifth International Conference on Tangible, Embedded, and Embodied Interaction* (Funchal, Portugal) *(TEI '11)*. Association for Computing Machinery, New York, NY, USA, 289–292. https://doi.org/10.1145/1935701.1935766

[84] Yujie Tao, Shan-Yuan Teng, and Pedro Lopes. 2021. Altering Perceived Softness of Real Rigid Objects by Restricting Fingerpad Deformation. In *The 34th Annual ACM Symposium on User Interface Software and Technology* (Virtual Event, USA) *(UIST '21)*. Association for Computing Machinery, New York, NY, USA, 985–996. https://doi.org/10.1145/3472749.3474800

[85] Cesar Torres, Tim Campbell, Neil Kumar, and Eric Paulos. 2015. HapticPrint: Designing Feel Aesthetics for Digital Fabrication. In *Proceedings of the 28th Annual ACM Symposium on User Interface Software and Technology* (Charlotte, NC, USA) *(UIST '15)*. Association for Computing Machinery, New York, NY, USA, 583–591. https://doi.org/10.1145/2807442.2807492

[86] Bernhard Treutwein. 1995. Adaptive psychophysical procedures. *Vision Research* 35, 17 (1995), 2503–2522. https://doi.org/10.1016/0042-6989(95)00016-X

[87] Bernard J Van der Horst, Maarten JA Duijndam, Myrna FM Ketels, Martine TJM Wilbers, Sandra A Zwijsen, and Astrid ML Kappers. 2008. Intramanual and intermanual transfer of the curvature aftereffect. *Experimental Brain Research* 187, 3 (2008), 491–496. https://doi.org/10.1007/s00221-008-1390-0

[88] Bernard J Van der Horst and Astrid ML Kappers. 2007. Curvature discrimination in various finger conditions. *Experimental brain research* 177, 3 (2007), 304–311. https://doi.org/10.1007/s00221-006-0670-9

[89] Bernard J van der Horst and Astrid M L Kappers. 2008. Haptic Curvature Comparison of Convex and Concave Shapes. *Perception* 37, 8 (2008), 1137–1151. https://doi.org/10.1068/p5780 arXiv:https://doi.org/10.1068/p5780 PMID: 18853551.

[90] Bernard J. van der Horst, Wouter P. Willebrands, and Astrid M.L. Kappers. 2008. Transfer of the curvature aftereffect in dynamic touch. *Neuropsychologia* 46, 12 (2008), 2966–2972. https://doi.org/10.1016/j.neuropsychologia.2008.06.003

[91] Marynel Vázquez, Eric Brockmeyer, Ruta Desai, Chris Harrison, and Scott E. Hudson. 2015. 3D Printing Pneumatic Device Controls with Variable Activation Force Capabilities. In *Proceedings of the 33rd Annual ACM Conference on Human Factors in Computing Systems* (Seoul, Republic of Korea) *(CHI '15)*. Association for Computing Machinery, New York, NY, USA, 1295–1304. https://doi.org/10.1145/2702123.2702569

[92] Ingrid M.L.C. Vogels, Astrid M.L. Kappers, and Jan J. Koenderink. 1999. Influence of shape on haptic curvature perception. *Acta Psychologica* 100, 3 (1999), 267–289. https://doi.org/10.1016/S0001-6918(98)00041-9

[93] Martin Weigel and Jürgen Steimle. 2017. DeformWear: Deformation Input on Tiny Wearable Devices. *Proc. ACM Interact. Mob. Wearable Ubiquitous Technol.* 1, 2, Article 28 (jun 2017), 23 pages. https://doi.org/10.1145/3090093

[94] Jacob O. Wobbrock, Leah Findlater, Darren Gergle, and James J. Higgins. 2011. The Aligned Rank Transform for Nonparametric Factorial Analyses Using Only Anova Procedures. In *Proceedings of the SIGCHI Conference on Human Factors in Computing Systems* (Vancouver, BC, Canada) *(CHI '11)*. Association for Computing Machinery, New York, NY, USA, 143–146. https://doi.org/10.1145/1978942.1978963

[95] Timothy H. Parker Wolfgang Forstmeier, Eric-Jan Wagenmakers. 2017. Detecting and avoiding likely false-positive findings – a practical guide. *Biological Reviews* 92 (November 2017), 1941–1968. Issue 4. https://doi.org/10.1111/brv.12315

[96] Munseok Yang and Junichi Yamaoka. 2022. MultiJam: Fabricating Jamming User Interface Using Multi-Material 3D Printing. In *Sixteenth International Conference on Tangible, Embedded, and Embodied Interaction* (Daejeon, Republic of Korea) *(TEI '22)*. Association for Computing Machinery, New York, NY, USA, Article 61, 5 pages. https://doi.org/10.1145/3490149.3505565

[97] Lining Yao, Ryuma Niiyama, Jifei Ou, Sean Follmer, Clark Della Silva, and Hiroshi Ishii. 2013. PneUI: Pneumatically Actuated Soft Composite Materials for Shape Changing Interfaces. In *Proceedings of the 26th Annual ACM Symposium on User Interface Software and Technology* (St. Andrews, Scotland, United Kingdom) *(UIST '13)*. Association for Computing Machinery, New York, NY, USA, 13–22. https://doi.org/10.1145/2501988.2502037

A DETAILED REPORTING OF THE POST-HOC TESTS RESULTS

We report detailed results of post-hoc tests in Tables 2 and 3. The '*' show significant differences confirmed by post-hoc tests.

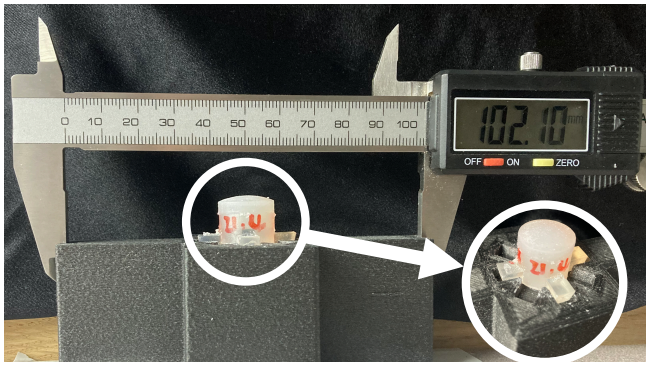

(a) A stimulus (Shore 00-10 R=21.4 mm) installed on 3D-printed support for the curvature measurement. A vernier scale is fixed on the support to make sure the precision of conversion of our measurement on pixels to mm.

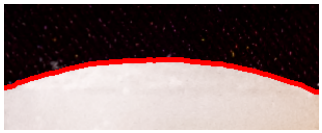

(b) A stimulus (Shore 00-10 R=21.4 mm) with edge detected, bolded and highlighted in red color for visualisation.

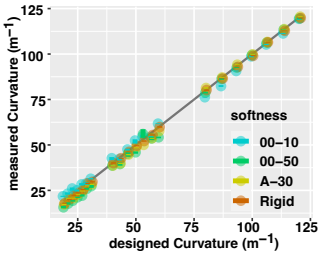

(c) The measured curvature of our stimuli vs. the designed curvature of our stimuli. Data points were slightly jittered horizontally avoid total overlap. The gray line indicates where the measured curvature equals the designed curvature.

Figure 11: Validation of the curvature of our stimuli.

B CURVATURE MEASUREMENTS

We verified the curvature of our stimuli as in [79]. We first took pictures of our stimuli (Figure 11(a)) with a Panasonic Lumix G Hybrides camera with a LUMIX G VARIO 14-140 lens (Focal length f=135 mm, resolution 1096× 2160). Pictures were calibrated to remove the distortion of the camera lens with OpenCV 4.6.0[8]. To ensure measurement accuracy, we took pictures of each stimulus from 8 angles (Figure 11(a) (bottom right)) by turning the stimulus around its axis in the placeholders, 3D printed in the support of the stimulus.

We then detected the contour of the curved surface of each stimulus with OpenCV. We fitted points to this contour (Figure 11(b)) using the circle-fit 0.1.3 [47] python package, to finally find its curvature (Figure 11(c)). To convert to curvature from pixels (px) to mm as shown in the y axis of Figure 11(c), we fixed a vernier scale on the support (Figure 11(a)) to ensure the precision of the conversion. We found that 102.10 mm on the scale equals 1945 px in the pictures. We therefore convert our measurements of the curvature with 0.053 mm/px. Figure 11(c) presents on the y-axis the results of our measurements with the average curvature of each stimulus and

[8] https://docs.opencv.org/4.x/

Table 2: Post-hoc tests of the impact of softness on precision (JND), accuracy, and subjective difficulty estimation.

R_{ref}	Softness pair (Shore)	Post-hoc test on precision				Post-hoc test on accuracy				Post-hoc test on difficulty			
		W	Z	p	r	W	Z	p	r	W	Z	p	r
10mm	00-10 vs. 00-50	37	-0.16	1	0.032	44	0.39	1	0.08	36	2.83	**<0.05***	0.58
	00-10 vs. A-30	54	1.18	1	0.24	66	2.12	0.21	0.43	45	2.88	**<0.05***	0.59
	00-10 vs. Rigid	53	1.10	1	0.22	63	1.89	0.32	0.38	55	3.02	**<0.05***	0.62
	00-50 vs. A-30	61	1.73	0.55	0.35	57	1.41	0.71	0.29	25	1.94	0.19	0.40
	00-50 vs. Rigid	51	0.94	1	0.19	53	1.10	0.90	0.22	45	2.92	**<0.05***	0.60
	A-30 vs. Rigid	51	-0.63	1	0.13	34	0.39	1	0.08	17.5	1.63	0.22	0.33
20mm	00-10 vs. 00-50	36	-0.24	1	0.05	42	0.24	1	0.05	61.5	2.68	**<0.05***	0.55
	00-10 vs. A-30	62	1.80	0.23	0.30	56	1.33	1	0.27	75.5	2.89	**<0.05***	0.59
	00-10 vs. Rigid	67	2.20	0.16	0.45	54	1.18	1	0.24	73	2.71	**<0.05***	0.55
	00-50 vs. A-30	65	2.04	0.21	0.42	55	1.26	1	0.26	41.5	2.37	0.07	0.48
	00-50 vs. Rigid	64	1.96	0.21	0.4	56	1.33	1	0.27	68	2.39	0.07	0.49
	A-30 vs. Rigid	41	0.16	1	0.03	28	-0.86	1	0.18	9	-0.64	0.69	0.13
40mm	00-10 vs. 00-50	40	0.59	0.59	0.12	37	-0.16	1	0.03	45	2.90	**<0.05***	0.59
	00-10 vs. A-30	63	1.88	0.19	0.38	54	1.17	1	0.24	57	2.18	0.15	0.44
	00-10 vs. Rigid	72	2.59	**<0.05***	0.53	53	1.10	1	0.23	54	2.74	**<0.05***	0.56
	00-50 vs. A-30	70	2.43	**<0.05***	0.50	61	1.73	0.55	0.35	21.5	0.60	0.63	0.12
	00-50 vs. Rigid	75	2.82	**<0.05***	0.58	51	0.94	1	0.19	53	1.89	0.19	0.39
	A-30 vs. Rigid	54	1.18	0.53	0.24	31	-0.62	1	0.13	32	2.14	0.19	0.44

Table 3: Post-hoc tests of the impact of softness on exploration time.

R_{ref}	Softness pair (Shore)	Post-hoc test on exploration time for first stimulus				Post-hoc test on exploration time for second stimulus				Post-hoc test on average exploration time			
		W	Z	p	r	W	Z	p	r	W	Z	p	r
10mm	00-10 vs. 00-50	49	0.78	1	0.16	38	-0.08	1	0.02	38	-0.08	1	0.016
	00-10 vs. A-30	54	1.18	1	0.24	53	1.10	1	0.22	56	1.33	0.81	0.27
	00-10 vs. Rigid	63	1.88	0.38	0.38	38	-0.08	1	0.02	62	1.80	0.46	0.37
	00-50 vs. A-30	46	0.55	1	0.11	56	1.33	1	0.27	59	1.57	0.65	0.32
	00-50 vs. Rigid	54	1.18	1	0.24	41	0.16	1	0.03	53	1.10	0.90	0.22
	A-30 vs. Rigid	36	-0.24	1	0.05	28	-0.86	1	0.18	37	-0.16	1	0.03
20mm	00-10 vs. 00-50	43	0.31	1	0.06	60	1.65	0.55	0.34	51	0.94	1	0.19
	00-10 vs. A-30	42	0.24	1	0.05	59	1.57	0.55	0.32	54	1.18	1	0.24
	00-10 vs. Rigid	57	1.41	1	0.29	75	2.82	**<0.05***	0.57	69	2.35	0.10	0.48
	00-50 vs. A-30	55	1.26	1	0.26	47	0.63	0.85	0.13	52	1.02	1	0.21
	00-50 vs. Rigid	48	0.71	1	0.14	54	1.18	0.80	0.24	48	0.71	1	0.14
	A-30 vs. Rigid	37	-0.16	1	0.03	50	0.86	0.85	0.18	43	0.31	1	0.06
40mm	00-10 vs. 00-50	62	1.80	0.39	0.37	66	2.12	0.17	0.43	63	1.88	0.32	0.38
	00-10 vs. A-30	61	1.73	0.39	0.35	66	2.12	0.17	0.43	62	1.80	0.32	0.37
	00-10 vs. Rigid	73	2.67	**<0.05***	0.54	75	2.82	**<0.05***	0.58	74	2.75	**<0.05***	0.56
	00-50 vs. A-30	41	0.16	1	0.03	48	0.71	1	0.14	42	0.24	0.85	0.05
	00-50 vs. Rigid	59	1.57	0.39	0.32	62	1.80	0.23	0.37	63	1.88	0.32	0.38
	A-30 vs. Rigid	47	0.63	1	0.13	46	0.55	1	0.11	52	1.02	0.68	0.21

respective 95% CI. The exact values of this graph and the code to compute the curvature are available in the supplementary material.